Experimental Neurology 329 (2020) 113288

Contents lists available at ScienceDirect

Experimental Neurology

journal homepage: www.elsevier.com/locate/yexnr

Research paper

Molecular profile of the rat peri-infarct region four days after stroke: Study with MANF

Jaakko Teppo[a,b], Anu Vaikkinen[a], Vassilis Stratoulias[b,c], Kert Mätlik[b], Jenni E. Anttila[b], Olli-Pekka Smolander[d], Päivi Pöhö[a], Brandon K. Harvey[e], Risto Kostiainen[a,*], Mikko Airavaara[b,c,*]

[a] Drug Research Program and Division of Pharmaceutical Chemistry and Technology, Faculty of Pharmacy, University of Helsinki, Finland
[b] Institute of Biotechnology, HiLIFE, University of Helsinki, Finland
[c] Neuroscience Center, HiLIFE, University of Helsinki, Finland
[d] Department of Chemistry and Biotechnology, Tallinn University of Technology, Estonia
[e] National Institute on Drug Abuse, IRP, NIH, Baltimore, MD, USA

ARTICLE INFO

Keywords:
Stroke
Peri-infarct
MANF
Transcriptomics
Proteomics
Metabolomics
Multiomics

ABSTRACT

The peri-infarct region after ischemic stroke is the anatomical location for many of the endogenous recovery processes; however, -the molecular events in the peri-infarct region remain poorly characterized. In this study, we examine the molecular profile of the peri-infarct region on post-stroke day four, a time when reparative processes are ongoing. We used a multiomics approach, involving RNA sequencing, and mass spectrometry-based proteomics and metabolomics to characterize molecular changes in the peri-infarct region. We also took advantage of our previously developed method to express transgenes in the peri-infarct region where self-complementary adeno-associated virus (AAV) vectors were injected into the brain parenchyma on post-stroke day 2. We have previously used this method to show that mesencephalic astrocyte-derived neurotrophic factor (MANF) enhances functional recovery from stroke and recruits phagocytic cells to the peri-infarct region. Here, we first analyzed the effects of stroke to the peri-infarct region on post-stroke day 4 in comparison to sham-operated animals, finding that strokeinduced changes in 3345 transcripts, 341 proteins, and 88 metabolites. We found that after stroke, genes related to inflammation, proliferation, apoptosis, and regeneration were upregulated, whereas genes encoding neuroactive ligand receptors and calcium-binding proteins were downregulated. In proteomics, we detected upregulation of proteins related to protein synthesis and downregulation of neuronal proteins. Metabolomic studies indicated that in after stroke tissue there is an increase in saccharides, sugar phosphates, ceramides and free fatty acids and a decrease of adenine, hypoxantine, adenosine and guanosine. We then compared the effects of post-stroke delivery of AAV1-MANF to AAV1-eGFP (enhanced green fluorescent protein). MANF administration increased the expression of 77 genes, most of which were related to immune response. In proteomics, MANF administration reduced S100A8 and S100A9 protein levels. In metabolomics, no significant differences between MANF and eGFP treatment were detected, but relative to sham surgery group, most of the changes in lipids were significant in the AAV-eGFP group only. This work describes the molecular profile of the peri-infarct region during recovery from ischemic stroke, and establishes a resource for further stroke studies. These results provide further support for parenchymal MANF as a modulator of phagocytic function.

1. Introduction

Stroke is the second most common cause of death and a significant cause of disability worldwide (Feigin et al., 2014). There are no pharmacological treatments for stroke besides thrombolysis with tissue plasminogen activators, which should be administered within hours from the ischemic stroke onset (Powers et al., 2018). While the majority of the patients survive, most require rehabilitation and complete functional recovery is unusual (Benjamin et al., 2019). Therefore, understanding the neurobiology of recovery and brain repair is important in order to develop drugs hastening the recovery from stroke. On the molecular level, multiple early mechanisms have been shown to play a

* Corresponding authors.
E-mail addresses: risto.kostiainen@helsinki.fi (R. Kostiainen), mikko.airavaara@helsinki.fi (M. Airavaara).

https://doi.org/10.1016/j.expneurol.2020.113288
Received 30 September 2019; Received in revised form 27 February 2020; Accepted 25 March 2020
Available online 27 March 2020

role in stroke-induced cell and tissue damage, including glutamatergic excitotoxicity, calcium dysregulation, oxidative stress, cortical spreading depolarizations, inflammation, and finally, cell death (Moskowitz et al., 2010). The apoptotic cell death ceases by the second day post-stroke, while by day 4, the endogenous recovery mechanisms are thought to be activated (Li et al., 2000; Liu et al., 2009; Mulcahy et al., 2003).

Upon ischemic stroke, the core of the ischemic lesion suffers from complete loss of blood flow, inducing necrosis within minutes. In contrast, in the peri-infarct region surrounding the core area, the tissue damage is less pronounced. The cellular events in the peri-infarct region are characterized by recruitment of neutrophils, which are subsequently replaced by increasing numbers of macrophages/microglia (Anttila et al., 2018; Gesuete et al., 2016; Rayasam et al., 2018). At the same time, reactive astrocytes start to accumulate in the peri-infarct area, leading to the formation of an astrocytic scar around the lesion core (Anttila et al., 2018). At the anatomical level, functional recovery from stroke can be due to neuronal rearrangement (plasticity) in the peri-infarct region or due to remodeling of neuronal connectivity in the contralateral hemisphere (Brown et al., 2009; Brown et al., 2007; Li and Murphy, 2008). Another brain repair mechanism can involve the migration of neural progenitors and their partial integration to the peri-infarct region (Liang et al., 2019). Nevertheless, the post-stroke peri-infarct region remains poorly characterized.

We have previously developed a method for targeting adeno-associated virus (AAV) vectors to the peri-infarct region and investigating the effect of local transgene expression on the post-stroke events in rats (Mätlik et al., 2014). By using this technique we found that ectopic expression of MANF in the peri-infarct area hastens the behavioral recovery after stroke as well as increases the number of phagocytic cells in the peri-infarct region (Mätlik et al., 2018). In addition, we have found MANF to be important for cortical development, neuronal extensions in differentiating cells, and modulating STAT3 phosphorylation in neurosphere cultures (Tseng et al., 2018; Tseng et al., 2017). However, the detailed mechanism of how MANF protects and restores the neurons in stroke is unclear. It seems likely that endogenous endoplasmic reticulum (ER) luminal MANF mediates proper protein folding (Yan et al., 2019), but the mechanism of MANF's action in the extracellular space remains unknown. While the plasma membrane receptor for extracellularly applied MANF remains elusive (Hellman et al., 2011), plasma membrane sulfatides have been indicated to bind MANF, inducing its cellular uptake (Bai et al., 2018).

The aim of this work was to study the molecular events occurring in the peri-infarct region during the initial phase of the recovery from ischemic stroke and to elucidate the effects of AAV-MANF treatment on these events. While individual omics technologies have been successfully applied to the study of brain tissue in stroke (Brea et al., 2015; Irie et al., 2014; Li et al., 2015), each technique has its limitations. Producing systems level information with multiple omics technologies poses a way to overcome these limitations. Using the distal middle cerebral artery occlusion (dMCAo) model of ischemic stroke in rats, followed by global, untargeted analysis of the transcriptome, proteome, and metabolome, we identified widespread changes induced by stroke, as expected, and immune response modulation by MANF. This is, to our knowledge, the first multiomics description of the molecular phenomena occurring in the ischemic peri-infarct area during the recovery from ischemic stroke, thus serving as a resource for future studies.

2. Materials and methods

2.1. Sample processing

The experimental design is presented in Fig. 1.

2.1.1. Animals

Male Sprague Dawley rats (age 7–8 weeks, weight 200–280 g, Envigo, Netherlands) were used. All animal experiments were conducted according to the 3R principles of EU directive 2010/63/EU on the care and use of experimental animals, local laws and regulations, and were approved by the national Animal Experiment Board of Finland (protocol approval number ESAVI/7812/04.10.07/2015). The animals were housed in groups of 4 with *ad libitum* access to food and water under a 12 h/12 h dark-light cycle and the well-being of the animals was monitored daily.

2.1.2. dMCAo and AAV injections

The right middle cerebral artery (MCA) and bilateral common carotid arteries (CCAs) were ligated as previously described (Airavaara et al., 2010; Airavaara et al., 2009; Mätlik et al., 2018; Mätlik et al., 2014). Briefly, rats were anesthetized with 4% chloral hydrate intraperitoneally (10 mL/kg, Sigma). CCAs were identified and isolated through a ventral midline cervical incision. A craniotomy was made on the right hemisphere and the distal branch of the right MCA was ligated with a 10–0 suture, followed by occlusion of CCAs with non-traumatic arterial clips. After 60 min, the suture around the MCA and arterial clips were removed. Body temperature of the animals was maintained at 37 °C. After recovery from anesthesia, the rats were returned to their home cage. The sham operated animals went through all the same procedures except the arteries were not ligated.

One day later, the neurological deficits of the stroke animals were evaluated with body asymmetry test and Bederson's score as previously described (Mätlik et al., 2018) and the rats were divided into equal groups to receive either AAV-MANF (human) or AAV-eGFP intracranial injections. On day 2 after dMCAo surgery, the animals were anesthetized with isoflurane and stereotaxic injections were performed as previously described (Mätlik et al., 2014). Briefly, 2.5 µL of AAV1-eGFP or AAV1-MANF was injected at a speed of 1 µL/min using a 10 µL Hamilton syringe with a 30-gauge blunt needle into two subcortical sites (A/P + 1.6, L/M + 2.2, D/V − 5.0 and A/P − 0.4, L/M + 4.0, D/V − 5.0). The needle was kept in place for 2 min after the injection to prevent backflow.

2.1.3. Sample collection

Two days after the AAV injections, rats were anesthetized by pentobarbital and perfused for 5 min with body temperature saline, brains were rapidly frozen in −50 °C isopentane and stored at −80 °C. The peri-infarct area was cryo-dissected with a punch as previously described (Airavaara et al., 2011). Unilateral tissue punches for the proteomic and metabolomics analysis from the peri-infarct region (approximate AP levels of +2 and + 0 mm) were taken from 1 mm coronal sections cut in a cryostat at −20 °C (Fig. 1). For the transcriptomic analysis, the samples were taken from the AP level + 1 from 1 mm coronal sections. The samples were kept frozen at −80 °C until subsequent transcriptomic, proteomic, and metabolomics processing. Proteomic and metabolomics analyses were performed on the same set of samples (N = 10, 9, and 11 for SHAM, AAV-eGFP, and AAV-MANF groups, respectively), whereas a separate set of samples was used for transcriptomics (N = 8 for all three sample groups).

2.1.4. Homogenization of samples for proteomics and metabolomics

The brain punch samples were thawed and weighed into tubes containing approximately 100 mg zirconia beads (1.0 mm diameter, BioSpec Products, Bartlesville, OK, USA). Tissue masses varied from 1.7 to 10.4 mg per sample. 30 µL of Milli-Q water per 1 mg of tissue was added, and the samples were homogenized with FastPrep-24 5G homogenizer (MP Biomedicals, LLC, Santa Ana, CA, USA) using one 40-s cycle with speed 6.0 m/s. The homogenates were centrifuged for 5 min at 8000 G at 4 °C to break the foam and stored at −80 °C. Samples were thawed and divided into three aliquots: one aliquot was used for positive ion mode metabolomics, one for negative ion mode metabolomics, and one for proteomics. Due to insufficient sample mass/volume, one AAV-MANF sample (C_11) and one SHAM sample

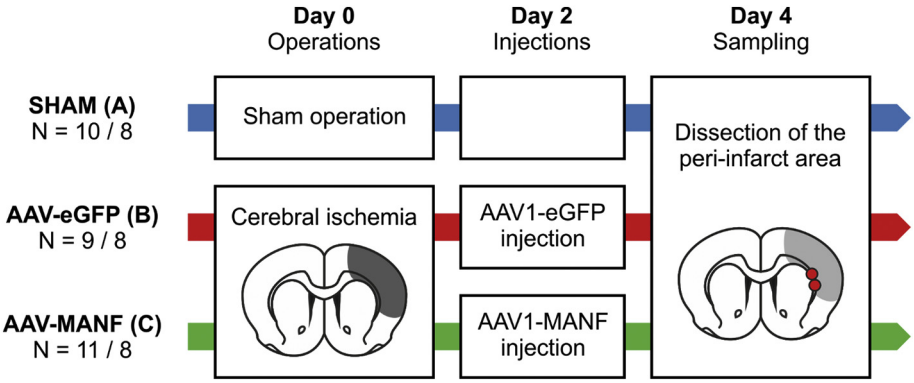

Fig. 1. Experimental outline. Male Sprague Dawley rats were subjected to 60 min cerebral ischemia or sham operation, followed by viral vector injections of MANF or eGFP 2 days post-stroke, and sampling of the peri-infarct area 4 days post-stroke. Numbers (N) correspond to animals used for proteomic and metabolomic / transcriptomic analyses.

(A_03) were not analyzed with the negative ion mode metabolomics method. One blank sample (6 µL of Milli-Q water) was processed like the brain samples and used in the metabolomics analysis (SP_blank, Data S3).

During homogenization, red hue indicating residual blood was observed in 12 samples by visual inspection (Fig. S1A). To account for the artifacts caused by the molecules from blood, the correlation of each protein and metabolite abundance with serum albumin is shown in the results using the color gradient presented in Fig. S1B, but no filtering of the results based on these correlations was applied (described in detail in the supplementary material).

2.2. Transcriptomics

2.2.1. Sample handling

RNA was extracted with Trizol reagent and treated with DNase (Ambion; #1906). Total RNA concentration and quality were determined with NanoDrop 1000 v3.7.1 and Agilent 2100 Bioanalyzer. Genomic DNA was removed from samples using Heat&Run gDNA removal kit, and cleanup and size selection (removal of small fragments) was done using Agencourt AMPure XP. rRNA was removed and the sequencing libraries were prepared using Illumina TruSeq Stranded Total RNA Library Prep Kit with Ribo-Zero Human/Mouse/Rat and sequenced on Illumina NextSeq 500 instrument using 75 bp kit.

2.2.2. Data processing

Adapter sequences and low quality reads were removed from the data using trimmomatic 0.36 (Bolger et al., 2014). Leftover rRNA reads were removed using SortMeRNA 2.1 (Kopylova et al., 2012). The data was mapped to *Rattus norvegicus* genome Rnor_6.0 using STAR 2.6.1d (Dobin et al., 2013). The original genome sequence and annotation was augmented with sequence and annotation for human *MANF* and *eGFP*. Count data was processed using GenomicFeatures 1.34.3 and GenomicAlignments 1.18.1 (Lawrence et al., 2013), and the differential expression analysis carried out using DESeq2 1.22.2 (Love et al., 2014). Changes with q-value < 0.01 and fold change > 2 were considered significant. Gene Ontology (GO) (The Gene Ontology Consortium, 2019; 2017) and Kyoto Encyclopedia of Genes and Genomes (KEGG) (Kanehisa and Goto, 2000) pathway enrichment analysis was performed with DAVID 6.8 (Huang et al., 2009a, 2009b), using the collapsed (DIR) GO terms.

The data have been deposited in the ArrayExpress database at EMBL-EBI (www.ebi.ac.uk/arrayexpress) under the accession number E-MTAB-8339.

2.2.3. Gene set enrichment analysis (GSEA)

For GSEA, we used minimally overlapping manually curated gene sets (suppl data table 'gene sets') based on transcriptomes of microglia, oligodendroglia, astrocytes, neurons, endothelial cells, and oligodendrocyte precursors from mouse cerebral cortex (Zhang et al., 2014) and mouse immune cell transcriptomes of macrophages from peritoneal cavity and granulocytes, dendritic cells, natural killer cells, B-2 B cells and T cells (not differentiating between CD4+, CD8+, T-reg and gamma delta T subtypes) from spleen (Gal-Oz et al., 2019). Gene counts from RNAseq analysis of SHAM, AAV1-eGFP, and AAV1-MANF samples were normalized with DESeq2 before running the analysis on GSEA 4.0.3 with 1000 permutations.

2.3. Proteomics

2.3.1. Sample preparation

20 µL of sample homogenate was used for proteomics. To solubilize the proteins, 100 µL of 0.2% (*w/v*) RapiGest SF in 50 mmol/L ammonium bicarbonate and 80 µL of 50 mmol/L ammonium bicarbonate were added to the samples, followed by 15 min sonication and 5 min heating to 99 °C with a heating block. Insoluble cell debris was removed by two 15-min rounds of centrifugation at 20817 G at 25 °C. Total protein content of the samples was determined using Thermo Pierce BCA Protein Assay Kit and the results were measured with CLARIOstar plate reader (BMG Labtech, Offenburg, Germany). The amount of homogenate equivalent to 46.5 µg of total protein was taken for further sample preparation and diluted to 200 µL with 0.1% (w/v) RapiGest SF in 50 mmol/L ammonium bicarbonate.

Disulphide bonds were reduced with 22 µL of 50 mmol/L dithiothreitol (final concentration 5 mmol/L) for 30 min at 56 °C and then carbamidomethylated with 25 µL of 150 mmol/L iodoacetamide (final concentration 15 mmol/L) for 30 min at room temperature and protected from light. Proteins were digested with 5 µL of 0.5 mg/mL sequencing grade modified trypsin overnight at 37 °C with shaking. Following digestion, the samples were acidified with 19 µL of 10% trifluoroacetic acid and the RapiGest SF was hydrolysed for 45 min at 37 °C, and consequently centrifuged for 10 min at 17949 G at 25 °C. 2.6 µL of acetonitrile was added to the samples, followed by purification with C18 MicroSpin columns (The Nest Group Inc., Southborough, MA, USA; SEM S118V) as previously described (Talman et al., 2018), evaporation to dryness with a vacuum centrifuge, and storage at −20 °C.

2.3.2. LC-MS analysis

Prior to LC-MS analysis, the samples were resolubilized in 30 µL of 0.1% trifluoroacetic acid, 1% acetonitrile in LC-MS grade water with 15 min sonication. The samples were analyzed in a randomized order, each sample followed by one wash run, and a pooled quality control (QC) sample was run at the beginning and the end of the sequence. The LC-MS analysis was performed with EASY-nLC 1000 coupled to Q Exactive mass spectrometer using Xcalibur version 3.1.66.10 (Thermo Scientific). Tryptic peptide solution equivalent to ~4.5 µg of digested protein (3.0 µL) was loaded onto Thermo Acclaim C18 columns (trap column: PepMap 100, 75 µm × 2 cm, 3 µm, 164,946; analytical column: PepMap RSLC, 75 µm × 15 cm, 2 µm, 164,940) and separated

using the following gradient: 5 min 5% eluent B, 120 min from 5 to 35% eluent B, 5 min from 35 to 80% eluent B, and 1 min from 80 to 100% eluent B, followed by 9 min column wash with 100% eluent B (A: 1% acetonitrile, 0.1% formic acid 0.01% trifluoroacetic acid in LC-MS grade water; B: 98% acetonitrile, 0.1% formic acid, 0.01% trifluoroacetic acid in LC-MS grade water). For detection, top10 data-dependent acquisition was applied, in which the 10 most intensive ions from the MS1 full scan (200 to 2000 *m/z*, resolution 70,000) were fragmented with collision-induced dissociation and analyzed in MS2 (isolation window 2 *m/z*, normalized collision energy 28, resolution 17,500). 30 s dynamic exclusion was applied.

2.3.3. Data processing

Protein identification (FDR < 0.01 on both peptide and protein level) and quantification were done with Andromeda and MaxQuant version 1.6.1.0 (Cox et al., 2011; Cox and Mann, 2008). Reviewed *Rattus norvegicus* UniProtKB/Swiss-Prot (UniProt Consortium, 2019) proteome (8023 entries, downloaded 2018-05-05), supplemented with separate fasta files for contaminants (embedded in MaxQuant), human MANF (accession P55145) and eGFP (accession C5MKY7), was used as the database, and the search was done with mass tolerance of 4.5 ppm in MS1 and 20 ppm in MS2. Protein quantification was done with unique and razor peptides, and LFQ (label-free quantification) intensity was used as a measure of protein abundance without further normalization.

Downstream data analysis was performed with RStudio (RStudio Team, 2019) version 1.1.456 running with R version 3.5.0 (R Core Team, 2019). Decoy hits and proteins flagged as potential contaminants were removed, excluding eGFP and porcine trypsin (accession P00761, used for QC). For statistical testing, missing values were imputed with normally distributed noise (mean = non-zero minimum for each protein divided by 10; sd = mean divided by 10). Protein LFQ intensities were compared with one-way ANOVA, Tukey's HSD *post-hoc* tests, and FDR multiple hypothesis correction; changes with q-value < 0.01 were considered significant. The enrichment analysis of GO (The Gene Ontology Consortium, 2019; 2017) terms and KEGG (Kanehisa and Goto, 2000) pathways was performed with DAVID 6.8 (Huang et al., 2009a, 2009b). For minimizing bias induced by the analytical method, the list of all quantified proteins was used as the background. Uncollapsed (ALL) GO terms were used. Trypsin, eGFP, and human MANF were excluded from the enrichment analyses.

Quality control data for the proteomics analysis is in the supplementary material. The data have been deposited in the MassIVE data repository (http://massive.ucsd.edu/) under the accession number MSV000083869.

2.4. Metabolomics

2.4.1. Extraction of metabolites

Extraction was performed for positive (POS) and negative ion mode (NEG) MS measurements separately as follows: 20 µL of homogenate or Milli-Q water (blanks, two for POS MS and three for NEG MS) was pipetted into an Eppendorf tube. 30 µL of Milli-Q water, 200 µL of methanol, and 5 µL of internal standard (IS) mixture were added to the tubes, and the tubes were vortexed. The POS MS IS mixture consisted of 4–20 µg/mL of d31-PC, d31-PG, lysoPC(17:0), 27-hydroxycholesterol-d6, verapamil, propranolol, d4-lysine, palmitic acid-d_{31}, ibuprofen, and pregnenolone-d4, and the NEG MS IS mixture of 25 µM d31-PG, 500 µM d4-lysine, and 500 µM palmitic acid-d_{31} in methanol. The tubes were transferred to ice and the samples were incubated for 30 min. Precipitate was removed by centrifugation at 12470 G for 5 min, and the supernatants were transferred into deactivated vial inserts for storage in −20 °C. A QC sample was prepared by pooling 5 µL of each sample extract.

2.4.2. LC-MS analyses

The analyses were performed with Thermo Dionex Ultimate 3000 UHPLC and Orbitrap Fusion mass spectrometer (Thermo Fisher Scientific). 5 µL (POS MS) or 3 µL (NEG MS) of sample was injected into a Waters Acquity BEH C18 column (2.1 × 100 mm, 1.7 µm particles) equipped with an in-line filter. For POS MS analysis, we used a 15-min linear gradient from 100% A to 100% B, followed by a 10-min isocratic period of 100% B, and a 5 min equilibration to initial conditions (A: 0.1% formic acid and 5% methanol in MQ water; B: 0.1% formic acid in methanol). Eluent flow rate was 0.30 mL/min. The column and autosampler temperatures were maintained at 25 and 10 °C, respectively. For NEG MS analysis, the separation was performed using a 3 min linear gradient from 30% to 90% B, followed by 1 min linear gradient to 100% B, 6 min isocratic period of 100% B, and 5 min equilibration to initial conditions (A: 6/94/1 volumetric ratio of methanol, Milli-Q water, and 1 mol/L NH_4COOH in Milli-Q water; B: 100/1 volumetric ratio of methanol and 1 mol/L NH_4COOH in MQ water). Eluent flow rate was 0.35 mL/min. The column and autosampler temperatures were maintained at 50 and 10 °C, respectively. Ionization was achieved with a heated electrospray source using the following settings (POS/NEG MS): spray voltage of 3.0/−1.9 kV, sheath gas 25/40 arbitrary units, auxiliary gas 10/12 arbitrary units, sweep gas 0/1 arbitrary units, ion transfer tube temperature 333 °C, and vaporizer temperature 290/317 °C. The data was collected in centroid mode. MS scans were performed with the resolution of 120,000 FWHM. In POS MS, the Easy-IC internal calibrant system of the MS instrument was used for internal calibration with fluoranthene. In NEG MS, the internal calibration system was not used. Data was collected at *m/z* range 100–1000 (POS MS, NEG MS 2–15 min), except at 0–2 min in NEG MS analysis, where *m/z* range 50–500 was collected in order to achieve sufficient sensitivity for small metabolites. The run order of samples was randomized except in the case of the QC sample and blanks. The QC sample was injected 6 times: as the first and last sample of the series and evenly distributed between samples. After initial data processing, MS/MS spectra were collected for the annotation of features with the largest fold changes (POS MS > 2, NEG MS > 1.5) and q < 0.01. For MS/MS, the individual samples in each sample group were pooled, resulting in one pooled sample per sample group. MS/MS data was acquired from the pooled sample with the highest MS1 signal. Quadrupole isolation window of 1, HCD fragmentation mode with energies of 25% and 40% and mass resolution of 30,000 FWHM were used for the MS/MS acquisitions.

2.4.3. Data processing

MzMine2 (Pluskal et al., 2010) was used for creating feature lists by applying the following functions: mass detection (centroid algorithm), chromatogram builder, chromatogram deconvolution (local minimum search algorithm), deisotoping, alignment (join aligner algorithm), filtering (number of found), gap filling, and filtering (duplicate filter). For POS MS data, peak areas were normalized with the average of relative responses of the internal standards d4-lysine, lysoPC(17:0), and d31-PC. For NEG MS data, peak heights were used without correction. Statistical tests were performed with RStudio (RStudio Team, 2019) (version 1.0.136/1.0.383 (POS/NEG MS)), running with R version 3.2.2 (R Core Team, 2019). Fold change values were calculated, and differences between the sample groups were searched with two-sided Student's *t*-test using Welch approximation. *p*-values were adjusted with FDR correction (Benjamini and Hochberg). Features with q < 0.01 and signal to noise > 5 in the upregulated group compared to blank samples were considered to have a statistically significant difference between the sample groups. Of these, features with fold change over 2 (POS MS) or 1.5 (NEG MS) were annotated based on the average accurate mass of the feature (from MzMine2 analysis) and by comparing the measured MS/MS spectra against spectral databases or repositories mzCloud (https://www.mzcloud.org/), NIST 2014 MS/MS (http://chemdata.nist.gov/), HMDB (Wishart et al., 2018), and Metlin (Guijas et al.,

Table 1
Primers used for the qPCR.

Gene	Forward primer	Reverse primer
Hprt1	CAGTCCCAGCGTCGTGATTA	TGGCCTCCCATCTCCTTCAT
S100a8	GAGTGCCCTCAGTTTGTGCAG	TCTGTTACTCCTTGTGGCTGTC
S100a9	CTGGAGCGCAGCATAAGCAC	GGTTTGTGTCCAGGTCCTCC

2018). In addition, literature (Pulfer and Murphy, 2003), CSI:FingerID (Dührkop et al., 2015; Shen et al., 2014), LipidMaps databases (Sud et al., 2007), and known group-specific fragmentation of lipids and phosphate groups containing species were used for the annotations. Some features were annotated as adducts or fragments based on accurate mass and retention time (and peak shape) matching that of a corresponding feature annotated by MS/MS. For selected lipids with corresponding accurate masses, same fatty acid composition was assumed in POS MS to that observed in NEG MS.

Quality control data for the metabolomics analysis can be found in the supplementary material.

2.5. Immunohistochemistry

Brain sections were deparaffinised and hydrated through xylenes and graded ethanol series and subjected to heat-induced antigen retrieval with 0.01 mol/L citrate buffer (pH 6.0) for 40 min using a steamer. For immunofluorescence, tissues were washed thoroughly with PBS, permeabilized with PBS-Triton-X 0.3% (*v*/v) and blocked with PBS-Triton-X 0.3% (v/v), 10% normal donkey serum. Next, tissues were incubated with primary antibodies overnight at 4 °C, washed thoroughly with PBS and incubated for 2 h with secondary antibodies. Tissues were counterstained with DAPI. The following primary antibodies were used sequentially: S100A9 (1/100; R&D systems, Cat# AF2065; RRID:AB_2184263), IBA1 (1/250; Cat# 019–19,741, RRID:AB_839504), donkey anti-goat 568 (Molecular Probes Cat# A-11057, RRID:AB_142581) and goat anti-rabbit 488 (Thermo Fisher Scientific Cat# A-11034, RRID:AB_2576217). Images were acquired with a Zeiss LSM700 confocal laser scanning microscope. For DAB staining and subsequent analysis, equivalent brain sections (number of animals per genotype = 7, number of sections per animal = 4) were deparaffinised and hydrated through xylenes and graded ethanol series and subjected to heat-induced antigen retrieval with 0.01 mol/L citrate buffer (pH 6.0) for 40 min using a steamer. Tissues were subsequently treated with 0.5% H_2O_2 for quenching of endogenous peroxidase activity for 30 min, washed with TBS, permeabilized with TBS-Triton-X 0.1% (v/v) and blocked with TBS-Triton-X 0.1% (v/v), 5% normal rabbit serum. S100A9 (R&D systems; Cat# AF2065, RRID:AB_2184263) primary antibody was diluted in blocking solution (1/1000) and tissues were incubated overnight at 4 °C. Next, sections were washed thoroughly with TBS and treated with anti-goat biotinylated antibody and avidin-biotin-peroxidase complex (PK-4005, Vector laboratories), and DAB substrate (SK-4100, Vector laboratories), according to manufacturer's instructions. Images were captured with a Pannoramic 250 FLASH II digital slide scanner (3DHISTECH) equipped with a 4MP CMOS camera. Images were analyzed using CaseViewer v.2.1 (3DHISTECH). Statistical analysis was performed with GraphPad Prism 6. Statistical analysis of the counts of S100A9-positive cells was done with unpaired two-tailed *t*-test.

2.6. qPCR

For qPCR, punch samples were used from the same animals as for proteomics and metabolomics, but using only 6 animals in the SHAM group. RNA was extracted from punch-samples of tissue, taken from the lateral peri-infarct cortex (AP level + 1 from a 1 mm coronal section cut in a cryostat). RNA was extracted with Trizol reagent and treated with DNase (Ambion; #1906). Total RNA concentration and quality were determined with NanoDrop 1000 v3.7.1 and Agilent 2100 Bioanalyzer. cDNA synthesis was carried out using an oligo-T18 primer and Maxima H minus reverse transcriptase (Thermo Fisher Scientific; #EP0751). Real-time quantitative PCR (qPCR) was performed on a Lightcycler®480 real-time PCR system (Roche Diagnostics) using Lightcycler®480 SYBR Green I Master complemented with 2.5 pmol of primers and cDNA corresponding to 10 ng of total RNA in the final volume of 10 µl on 384-well plates. Reactions were performed in duplicate and analyzed with Lightcycler®480 Software. The length of resulting PCR products was verified by agarose gel electrophoresis. Gene expression was normalized to rat Hypoxanthine guanine phosphoribosyl transferase 1 (Hprt1) expression level. Statistical comparison between the sample groups was done using one-way ANOVA with Tukey's multiple comparisons test. The primers are listed in Table 1.

3. Results

3.1. Transcriptomics

The peri-infarct region from rats subjected to stroke and treated with AAV-MANF or AAV-eGFP, and from sham operated rats, was analyzed (Fig. 1). We first carried out hierarchical clustering and principal component analysis (PCA) of the transcriptomics data. The SHAM group clearly separated from the stroke groups (AAV-eGFP and AAV-MANF), and the AAV-eGFP and AAV-MANF groups were similar (Fig. S2). One sample from the AAV-MANF group was characterized as an outlier based on inter- and intra-cluster distances and removed from the analysis. Altogether, 3347 genes were differentially expressed between the groups ($q < 0.01$, fold change > 2). The changes were remarkable in the comparison of stroke groups to the SHAM group, whereas there were only minor differences between the AAV-MANF and AAV-eGFP groups (Fig. 2A). In stroke samples compared to SHAM, more genes were upregulated than downregulated after stroke (Fig. 2A). Highly similar sets of transcripts were upregulated in the AAV-MANF and AAV-eGFP groups relative to the SHAM group, but the overlap was smaller in the downregulated genes (Fig. 2B). When comparing the AAV-MANF group to the AAV-eGFP group 77 genes were upregulated and 2 genes were downregulated. The majority of the differentially expressed genes were protein-coding (Fig. 2C). Enrichment analysis showed upregulation of genes related to inflammation, proliferation, apoptosis, and regeneration in the stroke groups relative to the SHAM group (Data S1). The raw and size factor normalized counts, ratios and q-values of the detected transcripts, the differentially expressed transcripts in each comparison, and the results of the enrichment analyses are listed in Data S1.

3.2. Proteomics

Altogether 2501 proteins were identified (FDR < 0.01 on peptide and protein level) and quantified. With hierarchical clustering and PCA, the SHAM samples were clearly distinguished from the other samples, but no differences were found between the AAV-MANF and AAV-eGFP groups (Fig. S3). Relative to the SHAM group, 308 (203 upregulated, 105 downregulated) and 213 (152 upregulated, 61 downregulated) proteins were differentially expressed in AAV-eGFP and AAV-MANF groups, respectively ($q < 0.01$, Fig. 3A and B). GO enrichment analysis showed upregulation of proteins related to protein synthesis and downregulation of neural proteins in both stroke groups relative to the SHAM group (enrichment analysis, Data S2). There was a high overlap between proteins differentially expressed in AAV-eGFP relative to SHAM and AAV-MANF relative to SHAM, and the overlap of the upregulated proteins was higher than that of the downregulated (Fig. 3B), as in transcriptomics. Only two proteins were significantly differentially expressed between the AAV-MANF and AAV-eGFP groups: S100A8 and S100A9 were downregulated in the AAV-MANF group (Fig. S4,

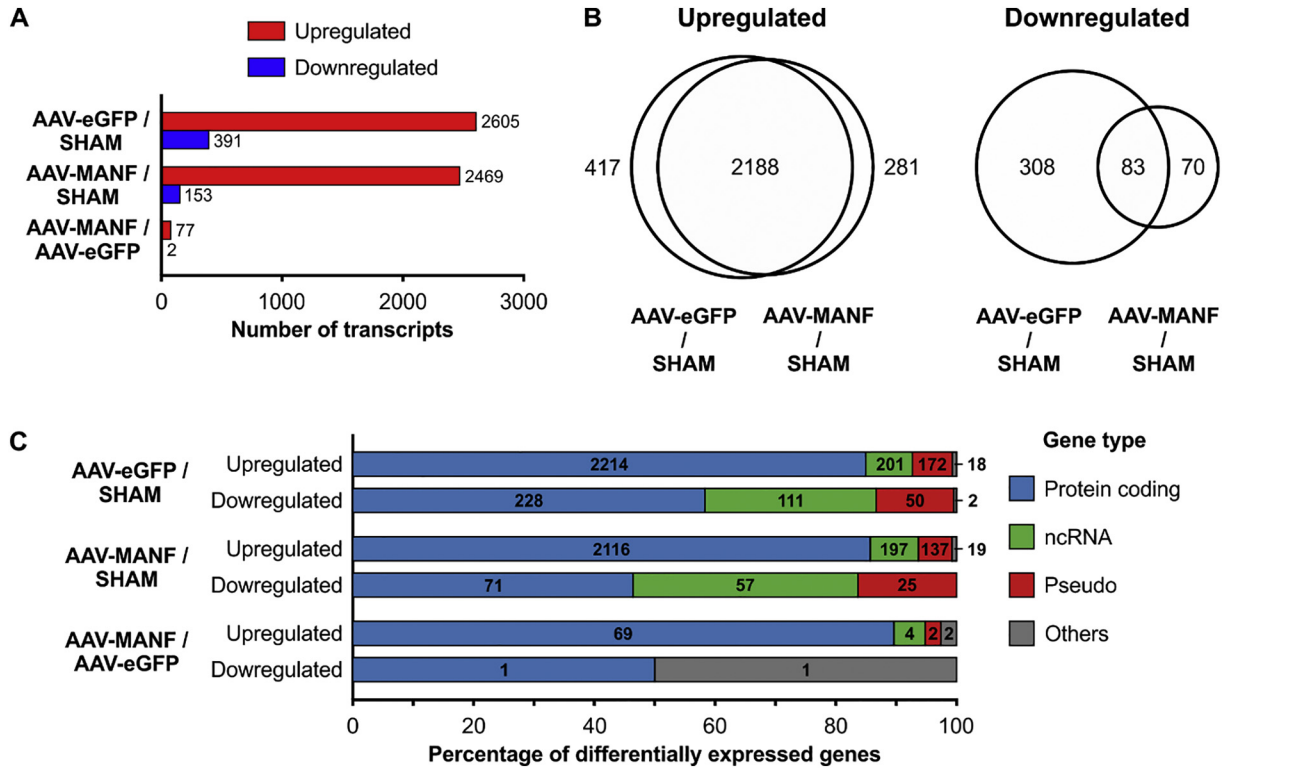

Fig. 2. A: Numbers of differentially regulated transcripts between the groups show major changes between the SHAM group and the AAV-eGFP or AAV-MANF groups, but minor changes between the AAV-eGFP and AAV-MANF groups. B: The ones upregulated are on the left and the ones downregulated are on the right C: Most of the transcriptomic changes occurred in protein-coding genes; gene type annotation according to NCBI Gene database (Brown et al., 2015), with the addition of AAV-expressed eGFP and hMANF to "others". A to C: criteria for significance were $q < 0.01$ and fold change > 2. (For interpretation of the references to colour in this figure legend, the reader is referred to the web version of this article.)

discussed in more detail in the MANF-induced changes). The LFQ intensities (raw and zero-imputed), ratios, and q-values of all quantified proteins, the differentially expressed proteins in each comparison, and the results of the enrichment analysis are listed in Data S2.

3.3. Metabolomics

The positive (POS) and negative (NEG) ion mode metabolomics analyses and data processing resulted in 7782 and 2001 features, respectively (Data S3). In line with transcriptomics and proteomics, PCA and hierarchical clustering of both the separate POS and NEG MS datasets showed separation of the SHAM group from the stroke groups (Figs. S5 and S6). The AAV-eGFP and AAV-MANF groups could not be separated from each other.

In positive ion mode, 95 and 65 features were lower in intensity in AAV-eGFP and AAV-MANF groups compared to SHAM, respectively, while 375 (AAV-eGFP) and 93 (AAV-MANF) features were higher in intensity ($q < 0.01$, fold change > 2, Fig. 4A). In negative ion mode, 46 and 27 features were lower in intensity in the AAV-eGFP and AAV-MANF groups compared to the SHAM group, respectively, while 111 (AAV-eGFP) and 26 (AAV-MANF) features were higher in intensity ($q < 0.01$, fold change > 1.5, Fig. 4B). Based on the MS/MS data and database/literature comparisons of these features, 88 metabolites with significantly different abundance between sample groups could be annotated (Fig. 4C and Data S3). Many of the annotated metabolites were seen as several features (total of 163 features assigned to the 88 metabolites) due to ionization in both POS and NEG MS, as well as in-source formation of adducts and fragments. No statistically significant differences were found between the AAV-eGFP and AAV-MANF groups, but for multiple metabolites, the changes relative to the SHAM group were significant in the AAV-eGFP group but not the AAV-MANF group. The annotated metabolite data and the unannotated feature data are listed in Data S3.

3.4. Stroke markers and transgene expression

Upregulation of the known stroke markers glial fibrillary acidic protein (GFAP) and heat shock protein beta-1 (HSPB1) on transcript and protein level was observed in both AAV-eGFP and AAV-MANF groups relative to the SHAM group, confirming successful infarction in the animals (Fig. 5A). In addition, the levels of acetylaspartic acid were decreased in the stroke samples, indicating neuron loss or dysfunction (Fig. 5B) (Demougeot et al., 2004; Moffett et al., 2007). As expected, the AAV1-expressed human Manf (*hManf*) and *eGFP* transcripts were heavily upregulated in the AAV-MANF and AAV-eGFP groups, respectively, and the human MANF and eGFP proteins were only detected in the corresponding groups (Figs. 5C and S7A).

Endogenous rat MANF protein was upregulated in the AAV-MANF group with $q < 0.01$ and in the AAV-eGFP group with $q = 0.019$ by about 2-fold relative to the SHAM group (Figs. 5C and S7A). MANF has been reported to be upregulated after stroke (Shen et al., 2012; Yu et al., 2010), but the slight difference in rat MANF levels observed between AAV-eGFP and AAV-MANF can be accounted for by the similar peptides in human and rat MANF (Fig. S7B; see the supplementary material for a detailed description). The levels of rat *Manf* transcript showed a trend towards upregulation in the stroke samples, but did not reach the significance criteria between the sham and stroke groups nor in the AAV-eGFP and AAV-MANF groups (Fig. 5C and S7A).

3.5. Stroke-induced changes

Next, the stroke-induced changes detected in the AAV-eGFP and/or AAV-MANF groups relative to the SHAM group were analyzed, characterizing the molecular profile of the post-stroke peri-infarct region.

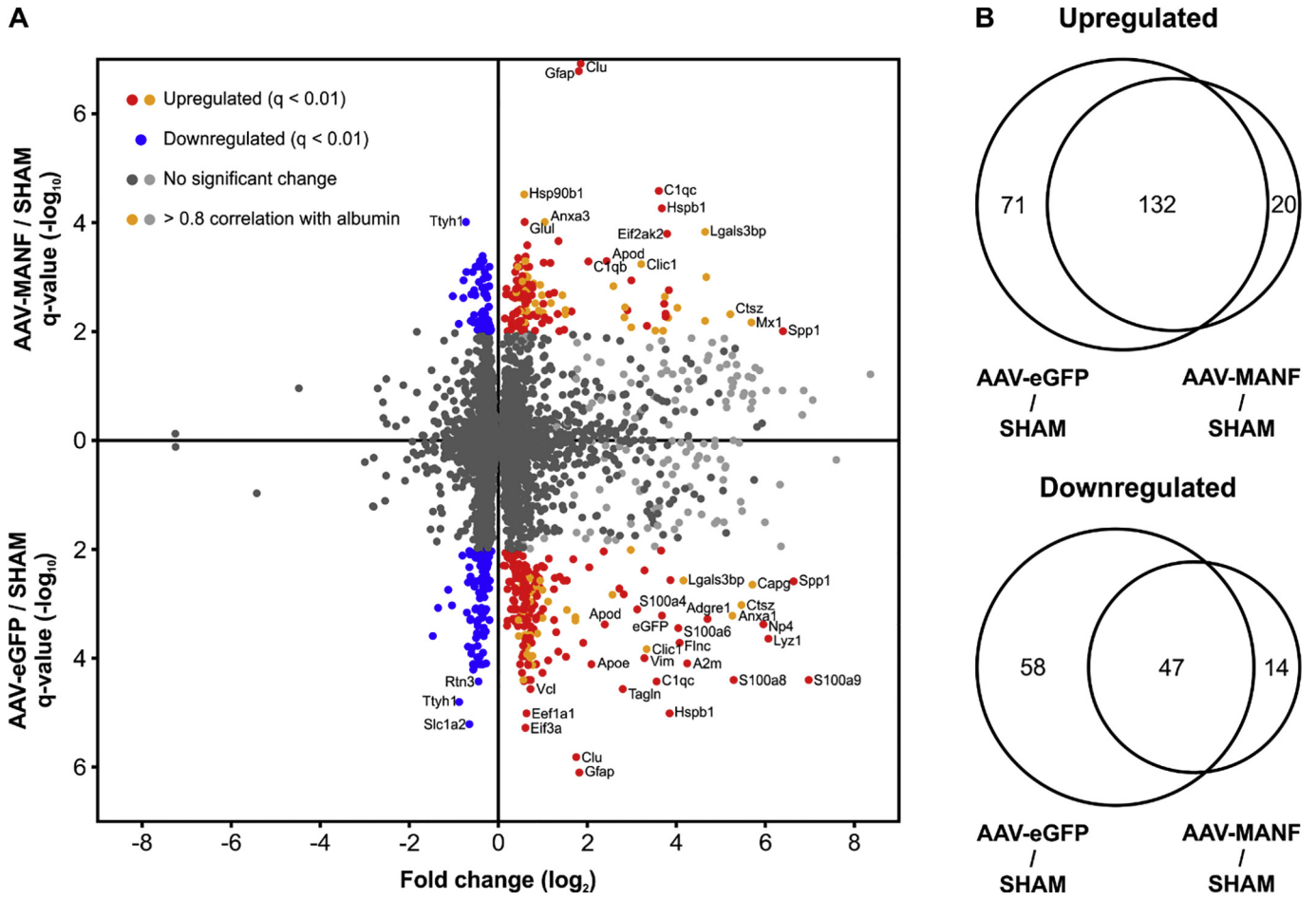

Fig. 3. A: Dual volcano plot showing the $\log_2$ fold changes and $-\log_{10}$ q-values of proteins in AAV-MANF/SHAM and AAV-eGFP/SHAM comparisons, calculated from the proteins' LFQ intensities. Overall, there are more changes, and the changes are larger and more significant, in the AAV-eGFP/SHAM comparison than in the AAV-MANF/SHAM comparison. Significantly upregulated and downregulated proteins are shown in colors. B: Venn diagrams showing the numbers of differentially expressed proteins in AAV-eGFP/SHAM and AAV-MANF/SHAM comparisons ($q < 0.01$; no fold change filtering), indicating higher overlap in the upregulated than in the downregulated proteins.

There was a remarkable overlap between the changes in the AAV-eGFP and AAV-MANF treated animals relative to SHAM (Figs. 2B, 3B, 4A, B), but relative to SHAM, there were multiple changes in the AAV-eGFP group that were not significant in the AAV-MANF group (Figs. 2A, 3A, 4C).

3.5.1. Energy metabolism

The levels of saccharides and sugar phosphates were increased in the stroke groups relative to the SHAM group, although for some saccharide species the increase in the AAV-MANF group was not statistically significant (Fig. 6A). On the proteomic level, no significant enrichment of energy metabolism-related pathways was observed, and the levels of enzymes catalyzing the rate-limiting steps of the KEGG pathways glycolysis/gluconeogenesis (rno00010), citrate cycle (rno00020), and oxidative phosphorylation (rno00190) were unchanged. On the transcriptomic level, no genes related to these three pathways changed significantly in expression. The proteins 6-phosphogluconate dehydrogenase, decarboxylating (PGD), and transaldolase (TALDO1), and the transcripts *Pgd*, deoxyribose-phosphate aldolase (*Dera*), and glucose-6-phosphate dehydrogenase (*G6pd*), in the pentose phosphate pathway (KEGG: rno00030), were upregulated in AAV-eGFP and/or AAV-MANF groups relative to the SHAM group (Fig. S8A), but no overall activation of the pentose phosphate pathway was observed.

3.5.2. Purine metabolism

In the metabolomics data, the levels of the purines adenine and hypoxanthine, and purine nucleosides adenosine and guanosine were decreased in the stroke groups relative to the SHAM group (Fig. 6B). Adenosine was significantly decreased in the AAV-eGFP group but did not reach statistical significance in the AAV-MANF group. A similar trend was found with guanine as well, although based on the metabolomics data, guanine can not be differentiated from a mass spectrometric fragment of guanosine. In contrast, the levels of the end product of purine degradation, uric acid, were increased in the AAV-eGFP group relative to the SHAM group, and the difference between the AAV-MANF and SHAM groups was not statistically significant. In line with this, the enzymes catalyzing the degradation of purines (Fig. 6B) were upregulated after stroke in the proteomics and/or the transcriptomics data (Fig. 6C). Other detected proteins than purine nucleoside phosphorylase (PNP) on the purine metabolism pathway (KEGG: rno00230) did not change in abundance, but some changes were observed in the transcriptomics data, mostly upregulation in the sample groups subjected to stroke (Fig. S8B). The decreasing nucleotide concentrations after stroke have been linked to reduced glucose-6-phosphate dehydrogenase activity (Irie et al., 2014), but in our data, the *G6pd* transcript was upregulated in AAV-eGFP group relative to SHAM, and the G6PDX protein showed no differences between the sample groups (Fig. S9B).

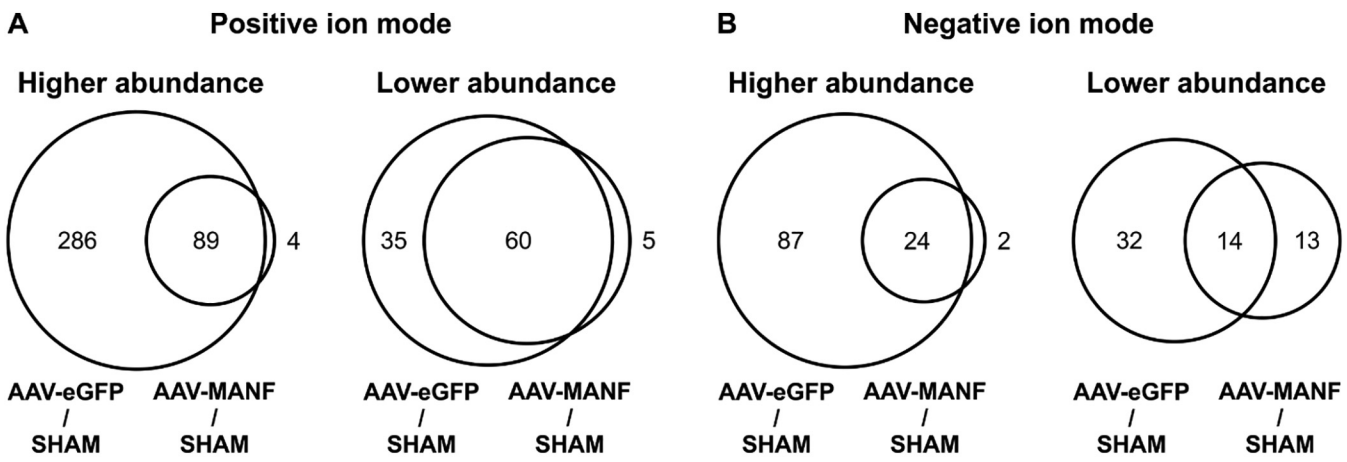

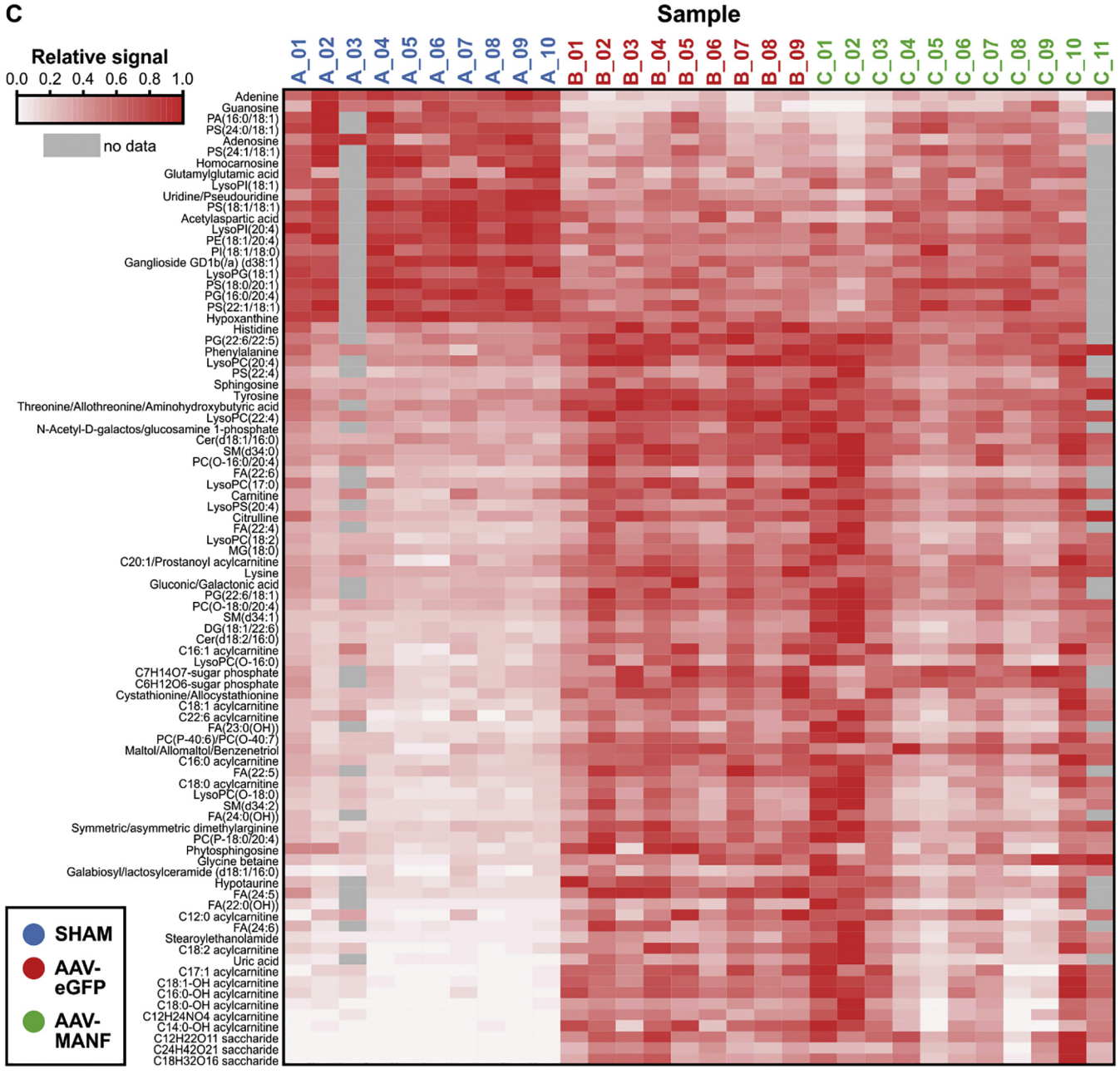

(caption on next page)

Fig. 4. (previous page). A and B: Venn diagrams showing the numbers of metabolomic LC-MS features of significantly different abundance in AAV-eGFP/SHAM and AAV-MANF/SHAM comparisons in positive (A) and negative (B) ion mode ($q < 0.01$; fold change > 2 in positive ion mode, > 1.5 in negative ion mode). C: Heatmap of the identified metabolites' relative signal across the samples.

3.5.3. Glutamatergic signaling

Glutamate-mediated excitotoxicity plays a major role in stroke (Lai et al., 2014), but as expected for samples collected 4 days post-stroke (Guyot et al., 2001), no change in glutamate levels was observed in the metabolomics data. No enrichment of genes related to glutamatergic signaling was observed in transcriptomics or proteomics (Data S1 and S2). However, glutamine synthetase (GLUL), the enzyme converting glutamate into glutamine, was upregulated in the stroke groups relative to the SHAM group (Fig. S8C). Also, aspartate aminotransferase, cytoplasmic (GOT1), the enzyme that biosynthesizes glutamate and oxaloacetate from 2-oxoglutarate and aspartate, was downregulated (Fig. S8C). The corresponding transcripts followed a similar pattern as the proteins, but their fold changes were below 2. The aforementioned metabolites, tentatively identified by exact mass, did not differ significantly between the sample groups and thus were not subjected to MS/MS for identification.

3.5.4. ER stress and unfolded protein response

Increased abundance of endoplasmic reticulum (ER) chaperone BiP (HSPA5) protein, and protein disulfide-isomerase (P4HB) protein and transcript, was observed in the stroke groups relative to the SHAM group (Fig. 7A), indicative of ER stress and the unfolded protein response (UPR). In line with this, an upregulation of proteins related to protein synthesis was observed in the stroke groups relative to the SHAM group (enrichment analysis, Data S2), but such enrichment of protein synthesis-related genes was not observed in the transcriptomics data.

3.5.5. Apoptosis/immune cells related markers

In the AAV-MANF and AAV-eGFP groups, we found upregulation of apoptosis regulator BAX in the proteomics data, BH3-interacting domain death agonist (*Bid*) in the transcriptomics data, and cathepsin D (CTSD) in both proteomics and transcriptomics data, because of immune cell infiltration (Fig. 7B). Also, the transcriptomics data showed an upregulation of genes related to NF-κB signaling in the stroke groups relative to SHAM (Data S1). Also, some transcripts of NF-κB subunits and NF-κB inhibiting proteins were upregulated (Fig. S9A), whereas the proteins were not detected. These changes are likely related to changes in cell type composition e.g. infiltration of immune cells after stroke. Furthermore, we detected upregulation of several caspase transcripts (Fig. S9B) and the enrichment of transcripts related to apoptosis (Data S1) in the stroke samples. Ceramides and other sphingolipids are known

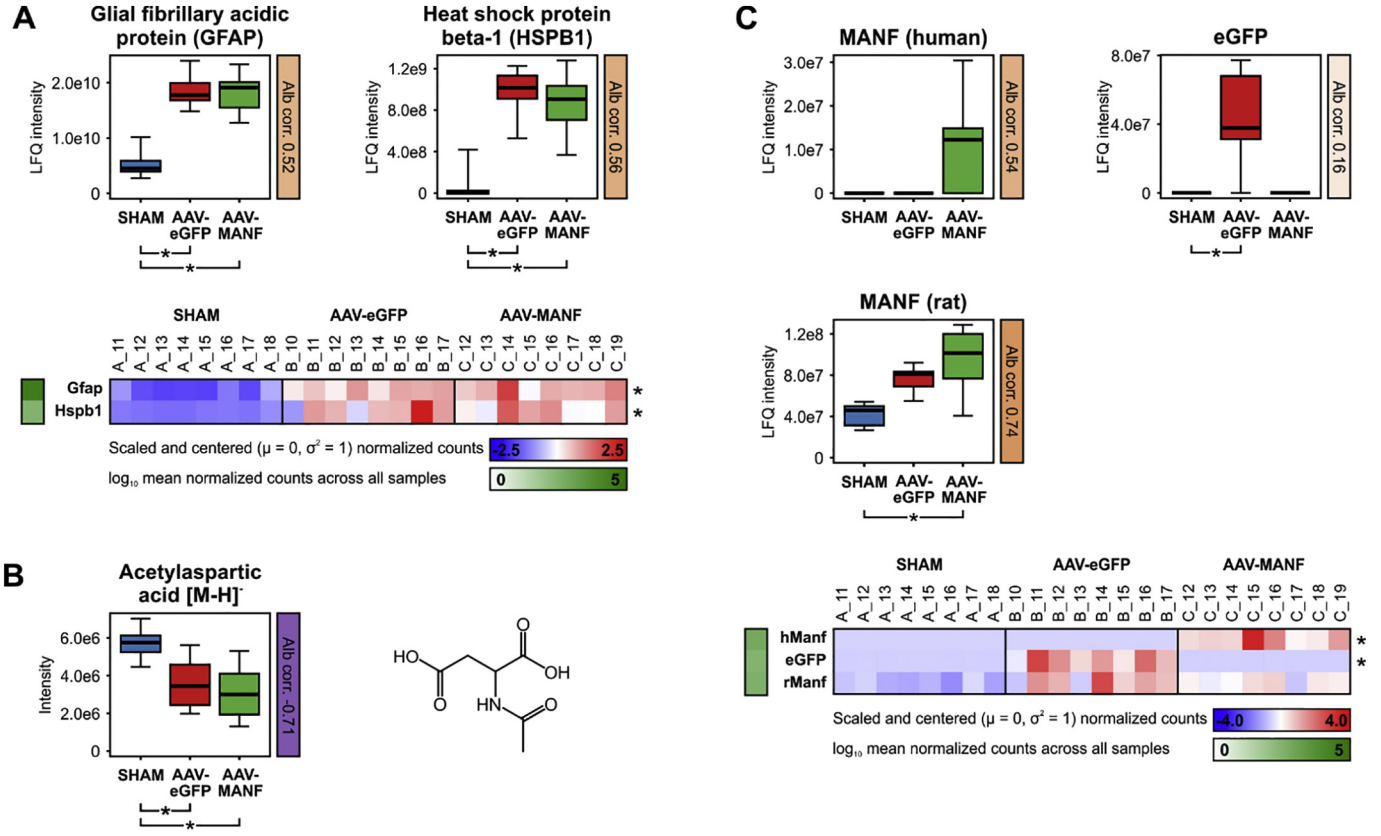

Fig. 5. A: Expression of the stroke markers GFAP and HSPB1, on protein (boxplots) and transcript (heatmap) levels, was increased in the sample groups subjected to stroke, confirming the validity of the dMCAo stroke model. B: Intensities of acetylaspartic acid decreased in sample groups subjected to stroke, indicating loss or dysfunction of neurons. C: Expression of the AAV1-expressed human MANF (*hManf*), enhanced green fluorescent protein (eGFP), and endogenous rat MANF (rManf), on protein (boxplots) and transcript (heatmap) levels. Increased transcript and protein abundance of the transgenes indicates successful transduction. Note that the eGFP protein appears to be significantly upregulated in the AAV-eGFP group compared to the SHAM group but not to the AAV-MANF group, although it was detected in neither the SHAM nor the AAV-MANF group; this is because in the FDR multiple hypothesis correction, the outcome q-values are affected not only by the number of statistical tests done, but also by the distribution of all uncorrected *p*-values (Benjamini and Hochberg, 1995). Asterisks indicate statistically significant differences in proteomics and metabolomics, and genes that were statistically significantly differentially expressed between any of the sample groups in transcriptomics. (For interpretation of the references to colour in this figure legend, the reader is referred to the web version of this article.)

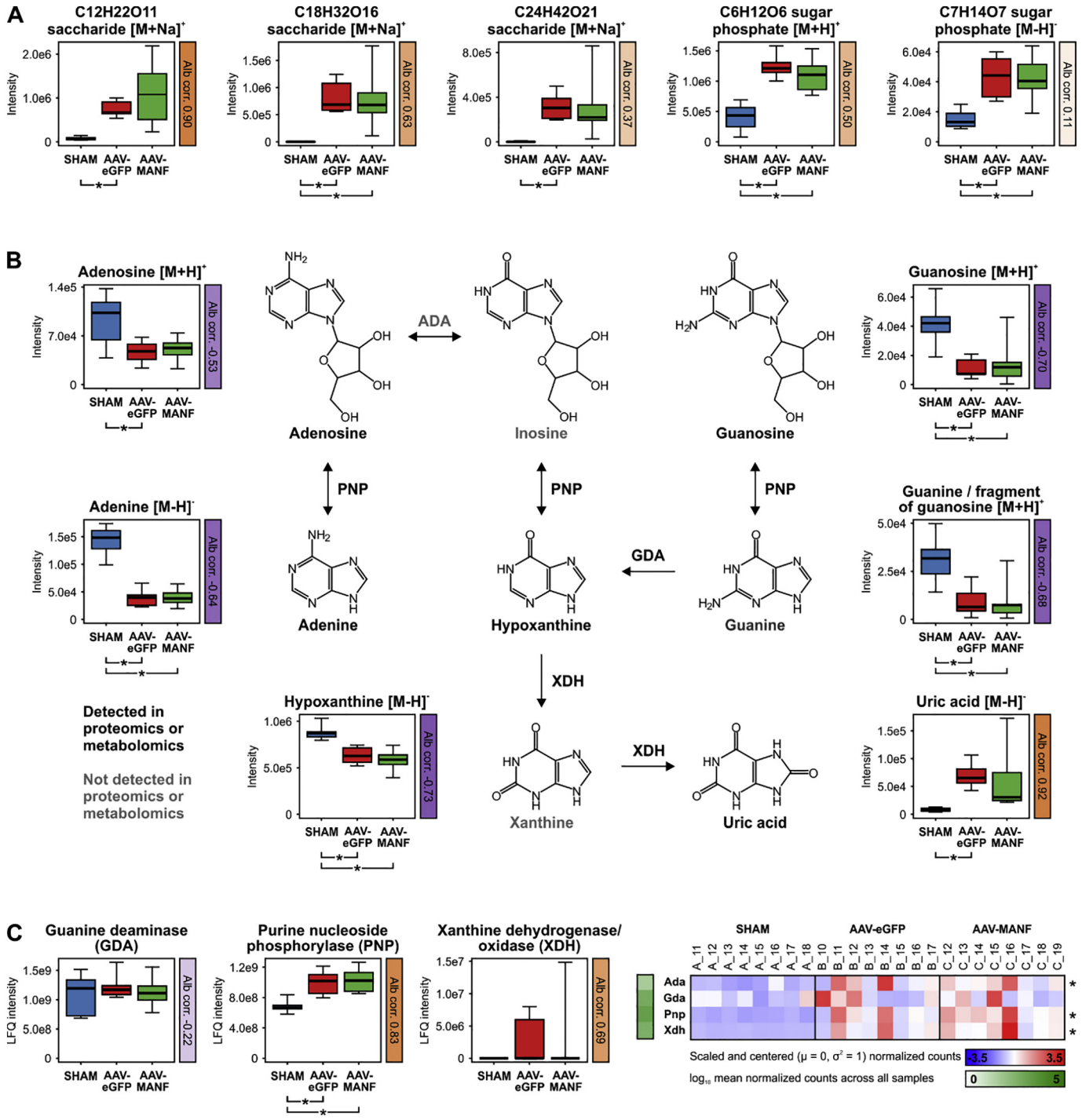

Fig. 6. A: Intensities of the detected saccharides and sugar phosphates increased in sample groups subjected to stroke. B: Part of the purine metabolism pathway and the intensities of the detected metabolites on the pathway, showing decrease of purine degradation reaction intermediates and accumulation of the end product, urate. C: Expression of the genes associated with the pathway part shown in panel B on protein (boxplots) and transcript (heatmap) levels, indicating activated purine metabolism.

to play a role in apoptosis (Taha et al., 2006), and in line with this, the metabolomics data showed approximately 2-fold increase of ceramide (d18:1/16:0) and ceramide(d18:2/16:0) in the AAV-eGFP group compared to the SHAM group, while for the AAV-MANF group there was a smaller increase and the q-value did not reach the < 0.01 level (Fig. 7C). Also, sphingosine and phytosphingosine (Fig. S9C), as well as the corresponding sphingomyelins (Fig. S9D) were increased in abundance in the AAV-eGFP group relative to the SHAM group. The transcriptomics data showed increased expression of several genes related to sphingolipid metabolism in the stroke groups relative to the SHAM group, but no significant changes in the detected corresponding proteins were seen (Fig. S9E). Changes in the levels of sphingosine-1-phosphate receptors were observed both in proteomics and transcriptomics (Fig. S9F), as another indication of infiltrating immune cells (Weigert et al., 2019).

3.5.6. *Phospholipase A2 activation*

One of the most prominent metabolic changes occurring after stroke

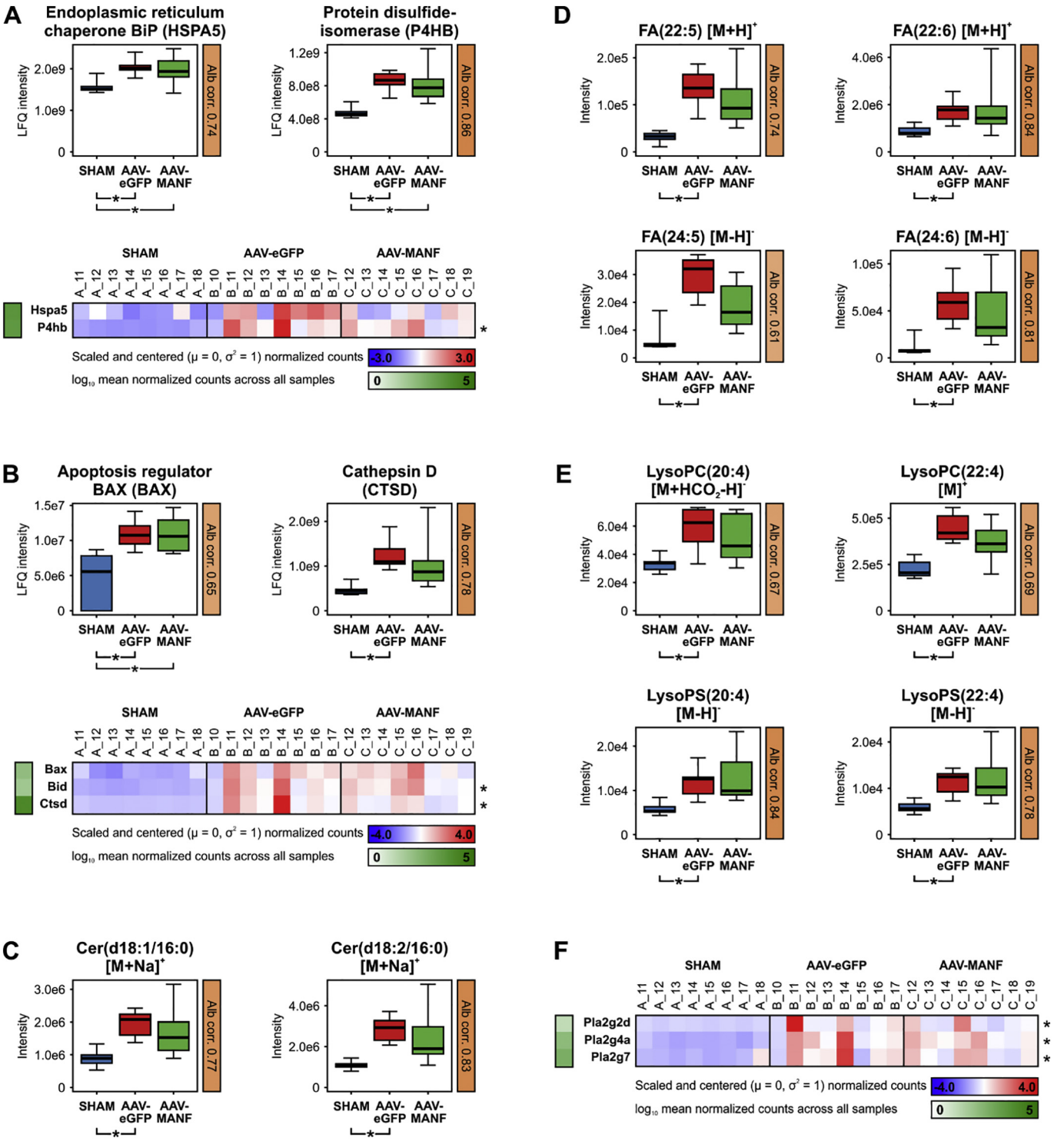

Fig. 7. A: Expression of ER stress markers HSPA5 and P4HB on protein (boxplots) and/or transcript (heatmap) levels increased after stroke. B: Increased expression *Bax*, *Bid*, and *Ctsd* on protein (boxplots) and/or transcript (heatmap) levels indicates infiltration of immune cells in the sample groups subjected to stroke. C to E: The intensities of certain ceramides (C), free fatty acids (D), and lysophosphatidylcholine and lysophosphatidylserine (lysoPC and lysoPS, respectively; E) lipid species were significantly increased in the AAV-eGFP but not in the AAV-MANF group relative to SHAM. F: In the sample groups subjected to stroke, the expression of three different phospholipase A_2 transcripts increased.

was the increase of free, long-chain unsaturated fatty acids; in most cases, the increase was significant in the AAV-eGFP but not in the AAV-MANF group (Fig. 7D). Acylcarnitines, the carnitine conjugates of fatty acids that enable the transport of fatty acids into mitochondria (Longo et al., 2016) and are potential stroke biomarkers (Seo et al., 2018), followed a similar pattern (Fig. S10A). In addition, a higher abundance of several lysophosphatidylcholine (lysoPC) and lysophosphatidylserine (lysoPS) lipid species were detected in the AAV-eGFP group than in the SHAM group; for the AAV-MANF group, the trend was similar, but the difference to the SHAM group did not reach statistical significance (Fig. 7E). The opposite behavior was observed for some lysophosphatidylinositol (lysoPI) and lysophosphatidylglycerol (lysoPG) lipid

species (Fig. S10B). Also, some phospholipid species decreased and others increased in abundance after stroke (Data S3), but our data does not show any systematic statistically significant decrease of certain phospholipid types (annotated by accurate mass only). hHowever, the trend was towards lower abundance in the stroke samples for most phosphatidylcholines, phosphatidylethanolamines, phosphatidylserines, and phosphatidylinositols.

Both free fatty acids and lysolipid species are cleaved from phospholipids by cytosolic phospholipase A_2 (cPLA$_2$). The transcriptomics data showed an upregulation of three PLA$_2$ genes after stroke: *Pla2g2d*, *Pla2g4a*, and *Pla2g7* (phospholipase A2, groups IID, IVA, and VII, respectively; Fig. 7F), but no enrichment of GO terms related to PLA$_2$ (Data S1). In the proteomics data, none of the PLA$_2$s were detected, but peroxiredoxin 6 (PRDX6), which in addition to its peroxidase activity displays calcium-independent PLA$_2$ (iPLA$_2$) activity, was slightly downregulated in the AAV-MANF group but not in the AAV-eGFP group relative to the SHAM group (Fig. S10C). PRDX6 overexpression downregulates TLR4 (Yeo et al., 2019), and in line with this, our transcriptomics data shows upregulation of *Tlr4* (Fig. S10C) and genes related to TLR signaling (enrichment analysis, Data S1) in the sample groups subjected to stroke. Furthermore, the proteomics data showed the upregulation of PLA$_2$ inhibiting proteins annexins A1 (ANXA1) and A5 (ANXA5) in the AAV-eGFP group and annexin A3 (ANXA3) in both the stroke groups relative to the SHAM group (Fig. S10D). In the transcriptomics data, annexins A1 to A5 were upregulated in the sample groups subjected to stroke.

3.6. MANF-induced changes

The MANF-induced changes detected between the AAV-eGFP and AAV-MANF groups are presented below, characterizing the effect of MANF treatment on the post-stroke peri-infarct region.

3.6.1. Response to virus

In transcriptomics data, 25 out of the 77 genes upregulated in the AAV-MANF group relative to the AAV-eGFP group were associated with GO terms indicating a response to the virus (Fig. 8A and B). Most of these genes were also upregulated in the AAV-eGFP group relative to the SHAM group (Data S1), but the upregulation was more pronounced in the AAV-MANF group. Of the proteins encoded by these genes, three were detected: interferon-induced GTP-binding proteins Mx1 and Mx2 (MX1 and MX2), and 2′-5′-oligoadenylate synthase 1A (OAS1A). MX1 was upregulated in the AAV-MANF group relative to the SHAM group, but no other changes were significant, although the trend was similar as in the transcriptomics data (Fig. 8C).

As MANF treatment seemed to modify the immune response towards the virus, we compared our data to a previous data set in which the transduction was done using AAV7 instead of AAV1 (Mätlik et al., 2018). In the stroke groups relative to SHAM, the changes in AAV7-transduced animals resembled those observed with AAV1, but in the AAV7-MANF to AAV7-eGFP comparison, no changes in response to virus-related transcripts was detected (Fig. 8D, Data S1). In the group-wise comparison between animals from the AAV1-treated and AAV7-treated sample sets, GO terms indicating a response to the virus were enriched only in the genes upregulated in AAV1-MANF relative to AAV7-MANF (Fig. 8E, Data S1), indicating a serotype-specific effect. In contrast, in the genes differentially expressed between the eGFP groups or the SHAM groups from these two sample sets, GO terms related to ribosome and protein synthesis were enriched.

We wanted to see whether the differences in gene expression point to a specific change in cell composition of the peri-infarct area after AAV1-MANF treatment. We performed Gene set enrichment analysis (GSEA) (Subramanian et al., 2005) to see whether there is a systematic change in the expression of genes that are expressed selectively or more highly in major brain cell types and blood-derived immune cells. As expected, compared to Sham-lesioned rats, the peri-infarct area of AAV1-GFP injected animals that had undergone dMCAo contained higher levels of mRNAs that are highly expressed in microglia and peripheral immune cells (Table S6A). Comparison of AAV1-MANF and AAV1-GFP-injected groups did not point to a clear change in cellular composition of the peri-infarct area (Table S6B).

3.6.2. Phagocyte recruitment

The proteins S100A8 and S100A9 that are highly expressed in macrophages and in neutrophils (Yui et al., 2003), were strikingly upregulated after stroke, but the effect was reversed by MANF expression (Figs. 9A and S4); these two proteins comprised the only proteins between the AAV-MANF and AAV-eGFP groups that reached the set criterion for statistical significance ($q < 0.01$). On the transcript level, the trend was similar: *S100a8* and *S100a9* were upregulated in the groups subjected to stroke, with more pronounced upregulation in the AAV-eGFP group than in the AAV-MANF group, but the difference between these two groups was not significant (Figs. 9B and S4). S100A8 and S100A9 induce proinflammatory cytokines via TLR4 and NF-κB, (Vogl et al., 2007), but in the transcriptomics data, genes related to these processes were upregulated in both stroke groups relative to SHAM, without any systematic difference between the AAV-MANF and AAV-eGFP groups (enrichment analysis, Data S1).

To further characterize the role of S100A8 and S100A9 in the peri-infarct region, we performed qPCR and immunohistochemistry. With qPCR, upregulation of the *S100a8* and *S100a9* transcripts was detected in the AAV-eGFP group but not the AAV-MANF group relative to SHAM (Fig. 9C). With immunohistochemistry, we were able to identify S100A9/IBA1 positive cells in the ipsilateral hemisphere in the stroke core and in the peri-infract area of animals treated with AAV7-MANF two days post-stroke (Fig. 9D and E). These cells were of amoeboid morphology and contained multiple nuclei (Fig. 9D, arrows), the latter being a feature of neutrophils and not of microglia. We also counted the number of S100A9-positive cells in the peri-infract area of animals subjected to stroke and subsequently treated with AAV7-GFP and AAV7-MANF, but no significant difference was observed (Fig. 9E and F).

4. Discussion

In this work, we characterized the transcriptomic, proteomic, and metabolomic fingerprint for the peri-infarct region four days after ischemic stroke in comparison to sham-operated rats. In addition, we investigated the molecular signature of post-stroke AAV-MANF treatment with AAV-eGFP as the control. We utilized a multiomics approach, in which the different omics techniques produce complementary information for a comprehensive picture. While transcriptomics provides a global picture of the mRNA levels, it misses the regulation of translation and variable protein turnover rates. Thus, protein abundance cannot be directly inferred from transcript abundance. On the other hand, both proteomics and metabolomics are biased towards molecules that are readily detectable with the liquid chromatography-mass spectrometry (LC-MS) instrumentation and the sample preparation methods used. Despite the high sensitivity of these instruments, many low-abundance proteins and metabolites are difficult to detect.

We identified both stroke-induced and MANF-induced changes in the peri-infarct region. Stroke caused changes related to metabolism and accumulation of sugars and sugar phosphates and purine degradation was increased. As expected, we detected markers of increased inflammation, ER stress, and apoptosis, as well as increased levels of various lipid classes, including free fatty acids, acylcarnitines, most sphingolipids, and some lysolipids. While the stroke-induced changes were remarkable, we did not find metabolomic changes induced by MANF, and the transcriptomic and proteomic changes were subtle. In an AAV1 vector, but not an AAV7 vector, MANF increased the expression of a number of genes related to defense response to a virus. We

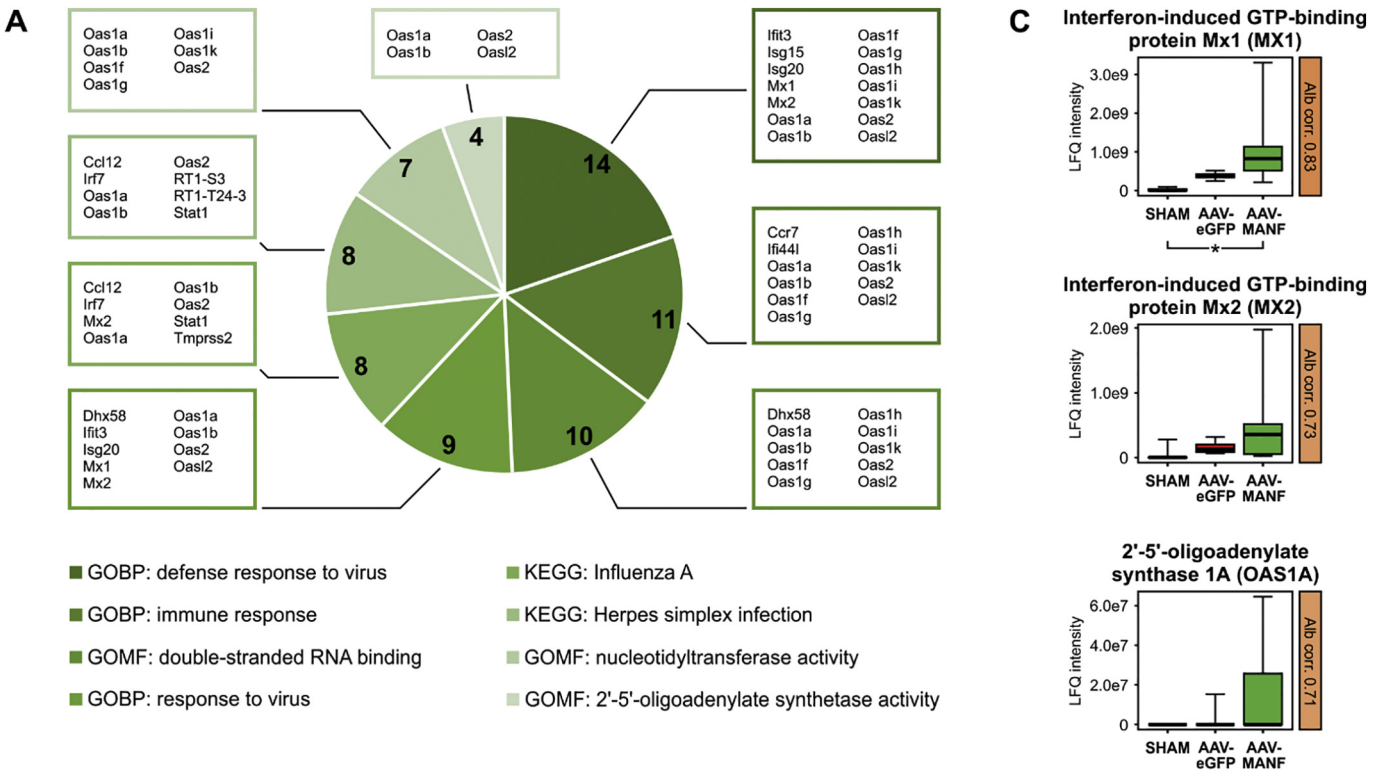

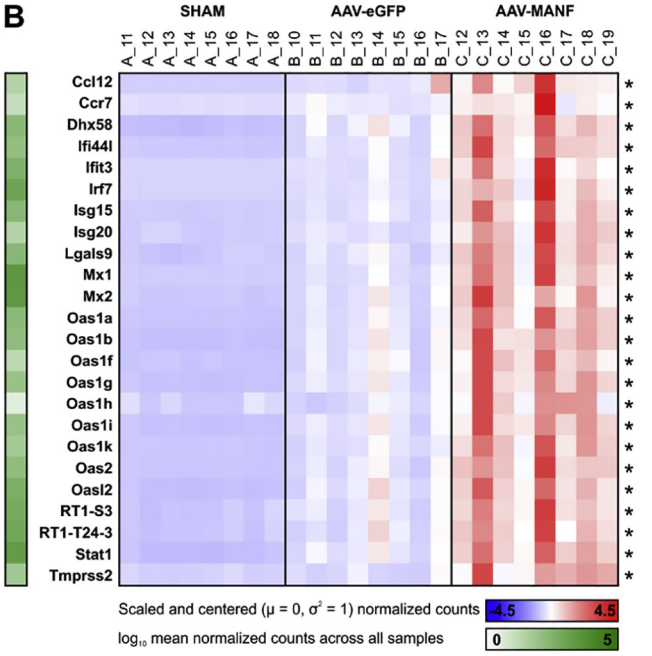

D

	Upregulated	Downregulated
AAV7-eGFP / SHAM	449 transcripts *inflammation, chemotaxis, regeneration*	46 transcripts *no significant enrichment*
AAV7-MANF / SHAM	489 transcripts *inflammation, chemotaxis, regeneration*	49 transcripts *no significant enrichment*
AAV7-MANF / AAV7-eGFP	2 transcripts *hManf, Adgre1*	1 transcript *LOC689935*

E

	Upregulated	Downregulated
SHAM: AAV1 / AAV7	2643 transcripts *genes encoding ribosomal proteins*	1165 transcripts *genes encoding ribosomal proteins*
AAV-eGFP: AAV1 / AAV7	2137 transcripts *genes encoding ribosomal proteins*	226 transcripts *genes encoding ribosomal proteins*
AAV-MANF: AAV1 / AAV7	2535 transcripts *response to virus, immune response*	756 transcripts *genes encoding ribosomal proteins*

Fig. 8. A: GO terms and KEGG pathways associated with immune response, especially to the virus, were significantly enriched in the genes upregulated in the AAV-MANF group relative to the AAV-eGFP group in transcriptomics. B and C: Expression of genes associated with defense response against virus on transcript (B) and protein (C) levels. Genes upregulated in the AAV-MANF group relative to the AAV-eGFP group in transcriptomics are shown. Asterisks indicate statistically significant differences in proteomics and metabolomics, and genes that were statistically significantly differentially expressed between any of the sample groups in transcriptomics. D: Summary of the transcriptomics changes detected when using AAV7 instead of AAV1 in a similar experimental design as described in Fig. 1. E: Summary of the transcriptomics changes detected between the animals treated with AAV1 and AAV7.

do not know why the AAV1 serotype combined with MANF caused this effect, while the GFP transgene did not. The difference may be due to tropism, and different serotypes may express MANF in different cell types and thereby contribute to a difference in the molecular changes. There may also be a difference in the transduction efficiency despite equivalent viral titers being injected into the brain. This would result in different effective doses of MANF to the brain. Additional studies beyond the scope of this investigation are needed to identify the reasons and one likely difference is the infiltration of inflammatory cells. Importantly, MANF reversed the stroke-induced upregulation of the

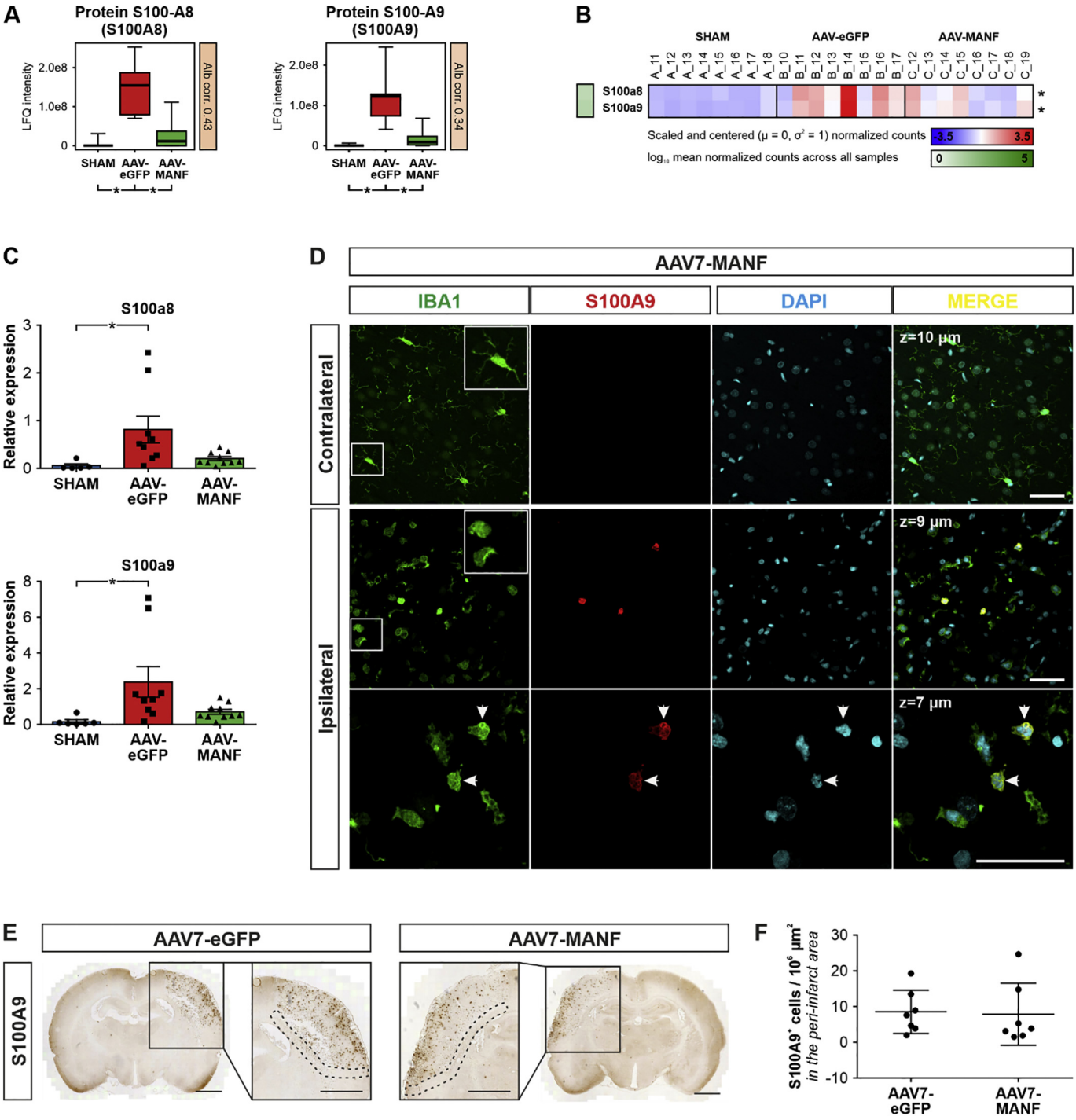

Fig. 9. A and B: Increased expression of proteins (A) and transcripts (B) of S100A8 and S100A9 after stroke is partially reversed by MANF treatment. C: qPCR of *S100a8* and *S100a9* transcripts shows similar changes as detected with proteomics and RNA sequencing (mean ± s.e.m., one-way ANOVA with Tukey's multiple comparisons test). D: S100A9-positive cells are detected in the ipsilateral side of 4-day post-stroke rats treated with AAV7-MANF. These cells are also positive for the myeloid marker IBA1 and contain multiple nuclei (arrows). White squares (top right) correspond to magnification of white squares at the left side of image. Scale bars, 50 μm. E: S100A9-positive cells are found both inside the ischemic core and in the peri-infarct area of both AAV7-eGFP and AAV7-MANF treated animals. Scale bars, 2000 μm. F: Statistical analysis of S100A9-positive cells found in the peri-infract area of AAV7-eGFP and AAV7-MANF treated animals (mean ± s.e.m., unpaired two-tailed *t*-test).

phagocyte proteins S100A8 and S100A9. The effect was validated on the transcript level with qPCR, and with immunohistochemistry where S100A9 was mapped to cells with the morphology of neutrophils.

In ischemic stroke, the oxygen and glucose deprivation leads to an energy failure that induces widespread effects in the tissue. As no changes in the expression of energy metabolic enzymes were detected in our data, the increased levels of saccharides and sugar phosphates in the stroke samples (Fig. 6A) may suggest attenuation of energy metabolism and the consequent accumulation of upstream energy metabolism precursors. Pentose phosphate pathway activation during cerebral ischemia has been reported (Imahori et al., 2017), but our data suggests that the activation is resolved by four days post-stroke (Fig. S8A).

Activation of purine degradation after stroke was observed in all omics levels (Fig. 6B and C). In hypoxic conditions, ATP

dephosphorylation into adenosine continues and, at the same time, adenosine kinase is not able to compensate for the loss of ATP. Thus, intracellular levels of adenosine increase, resulting in its release into the extracellular space (Van Wylen et al., 1986) and/or catabolism. ATP is replenished by recirculation at reoxygenation, and adenosine levels of the cerebral interstitial fluid decrease to baseline within 20 min after the hypoxic incident. Similar release of guanosine has also been reported, although the degradation of guanosine is not as rapid as that for adenosine, and guanosine levels in the ischemic tissue have been found to be increased at 7 days after ischemia but decrease to normal levels by 21 days after ischemia (Uemura et al., 1991). In our data, the levels of adenosine and guanosine in the peri-infarct region tissue were decreased from the baseline (SHAM group) 4 days post-stroke (AAV-eGFP and AAV-MANF groups) (Fig. 6B). This appears to be in disagreement with the cited report, in which guanosine levels were increased at 7 days post-stroke (Uemura et al., 1991); however, in that study, the infarct volume was sampled, whereas ours concentrated on the peri-infarct region. On the other hand, the accumulation of uric acid is in line with our results (Fig. 6B). Uric acid appears to play a role in stroke, although its exact function in stroke is unclear (Pello et al., 2009).

A similar observation of decreasing nucleotide concentration has been reported before (Irie et al., 2014), and it was suggested that this may be due to the reduced activity of glucose-6-phosphate dehydrogenase (*G6pd* or G6PDX) in the pentose phosphate pathway. Our data does not support this, as this enzyme showed a trend towards upregulation in the stroke samples (Fig. S8A). However, the activity of the human homologue of G6PDX is controlled by *N*-acetylation (Wang et al., 2014), and if this applies to the rat homologue as well, abundance alone is not sufficient to explain the potential changes in G6PDX activity. Protein *N*-acetylation was not investigated in our study. Importantly, the dual-function enzyme xanthine dehydrogenase/oxidase (XDH), that catalyzes the reaction in which hypoxanthine is transformed into xanthine and further into uric acid, has been reported to be converted into its reactive oxygen species-producing oxidase form during ischemia (Kinuta et al., 1989), and may be involved with the oxidative damage to the ischemic tissue.

The UPR is a protective mechanism for cells against increased misfolding of proteins in the lumen of the ER (Oslowski and Urano, 2011). In the stroke groups, we detected an increase of ER stress markers in the transcriptomic and proteomic data (Fig. 7A) whereas MANF levels were increased only at the protein level. However, we did not observe an increase in the common markers of the three UPR arms e.g. sXbp1, ATF6 or ATF4, although MANF protein levels have been shown to be increased by various ER stressors. It has been indicated that ER stress is associated with ischemia (Hadley et al., 2018; Yang and Paschen, 2016) and ER stress can be activated by oxidative stress, characteristic of the ischemia/reperfusion of the dMCAo stroke model, and ER stress and oxidative stress act in synergy and potentiate each other (Nakka et al., 2016). However, we measured the levels at day four post-stroke, indicating that global ER stress is transient. MANF plays a role in the UPR, as evidenced by the activation of the UPR in MANF knockout models, its protective effect against ER stress-induced cell death, and its upregulation and secretion in ER stress (Apostolou et al., 2008; Lindahl et al., 2014; Tseng et al., 2017). MANF-induced changes related to the UPR or ER stress were not detected in our study, but that could be related to time-dependent changes in the UPR following stroke (Morimoto et al., 2007).

Although apoptotic cell death has been reported to cease by 2 days post-stroke at the cellular level (Li et al., 2000; Liu et al., 2009; Mulcahy et al., 2003), our data indicate increase in markers of apoptotic activity still at 4 days post-stroke. We found increased expression of *Ctsd*, *Bid*, and *Bax* proteins/transcripts, and caspase upregulation (Fig. 7B, C, and S9B, respectively). Although these are associated with apoptosis they can also have other functions in the cells, e.g. caspases and BAX have been shown to be involved in long-term depression (Jiao and Li, 2011), caspases are activated in myeloid cells after stroke (Rodhe et al., 2016). Cathepsin-D is a protease enzyme that is active in lysosomes, and *Ctsd* and *Bid* are rather specific for microglia/macrophages. Several studies have previously reported increase of ceramides in stroke (Yu et al., 2007), and ceramides, specifically ceramide (16:0), have been found to induce apoptosis in several different types of stress models (Taha et al., 2006). The route of accumulation of ceramide in stroke is unclear, since evidence of both *de novo* synthesis and breakdown of sphingomyelin has been found, and our data on this is inconclusive: upstream components of ceramide biosynthesis were not detected, sphingomyelins followed a similar abundance pattern as ceramides (Fig. S9D), and the enzymes catalyzing the ceramide-producing reactions retained constant levels. Also, the upregulation of *Ctsd*, *Bid*, and *Bax* transcripts and/or proteins points towards lysosomal degradation and extracellular receptor activation as initiators of ceramide-related apoptotic events (Kashkar et al., 2005). In these pathways, sphingomyelinases produce ceramide that activates CTSD, which in turn activates BID that acts on BAX.

Notably, for ceramides, sphingosine and phytosphingosine, and the corresponding sphingomyelins (Figs. 7C, S9C, and S9D, respectively), the abundance increase relative to SHAM was significant in the AAV-eGFP group but not the AAV-MANF group, possibly pointing towards a MANF-induced effect that was too small or variable to reach statistical significance. A similar trend also applied to free fatty acids and lysoPC and lysoPS lipid species (Fig. 7D and E), of which the lysoPSs have immunomodulatory roles (Frasch and Bratton, 2012; Kamat et al., 2015). Previous work has found free fatty acids, including arachidonic acid (ArAc, FA(20:4)), to be increased in the early stage of ischemia/reperfusion (Narita et al., 2000; Yang et al., 2017; Yoshida et al., 1980), but the levels seem to return to baseline after 2–6 h after the onset of MCAO. Increase of docosahexaenoic acid (DHA, FA(22:6)) occurs later and its levels are above baseline at least a day after the MCAO onset (Narita et al., 2000; Yang et al., 2017). Our data is in agreement with these findings, as at the studied day 4 time point FA(22:6) was up over 2-fold (Fig. 7D), but FA(20:4) was increased only by approximately 20% after stroke without statistical significance (data not shown).

The origin for the increase of the free fatty acids and lysolipids in the brain after stroke is unclear. One possible explanation is PLA_2 that catalyzes the production of free fatty acids and lysophospholipids by cleaving fatty acids from the sn-2 position of various phospholipids. The increased free fatty acid, lysoPC, and lysoPS abundance, together with the trend towards decreased abundance of most phospholipids, suggests that the free fatty acids originate from phosphatidylcholine (PC) and phosphatidylserine (PS) lipid species (Fig. 7D and E). The exact subtypes of activated PLA_2s have not been confirmed, leaving some uncertainty of the cleaved phospholipid classes. The increased abundance of *Pla2g2d*, *Pla2g4a*, and *Pla2g7* transcripts (Fig. 7F) suggests increased expression of these subtypes, but cannot be confirmed, since none of the PLA_2 proteins were detected. PLA_2 activation that results from the calcium influx occurring at the onset of ischemia is a well-reported phenomenon (Adibhatla et al., 2006). In addition, the calcium influx promotes ER stress (Krebs et al., 2015) and can trigger calcium release from the ER (Bootman et al., 2002), which may potentiate or prolong the PLA_2 activity. It is possible that the PRDX6 downregulation (although the PLA_2 activity of PRDX6 is calcium-independent; Fig. S10C) and upregulation of PLA_2-inhibiting annexins (Fig. S10D) observed in our data represent a negative feedback-type PLA_2 silencing function which is activated as a response to stroke and remains active at least 4 days post-stroke. Notably, the $iPLA_2$ activity of PRDX6 mediates inflammation in cerebral ischemia/reperfusion (Shanshan et al., 2017).

It is also possible that the free fatty acids originate from circulation. Since the blood-brain barrier is known to be damaged in ischemia and thus permeate serum albumin (Abdullahi et al., 2018; Merali et al., 2017), the increase of free fatty acids may be due to albumin-bound fatty acids. Indeed, many of the free fatty acids, as well as various other lipid species, had moderate to high correlation with albumin. Notably, intravenously administered albumin-bound FA(22:6) has been shown to

be neuroprotective after stroke (Eady et al., 2014; Eady et al., 2012). In hemorrhagic stroke, MANF has been suggested to mediate its neuroprotective effects partially by defending the blood-brain barrier integrity (Li et al., 2019), but our data shows no evidence of this, likely because of the late administration of MANF: there was no difference in the albumin levels between the AAV-MANF and AAV-eGFP groups, indicating no difference in blood-brain barrier permeability (Fig. S1A).

Compared to the stroke-induced changes, the changes due to MANF treatment were more subtle. In transcriptomics, we detected increased immune response towards the virus in the AAV-MANF group relative to the AAV-eGFP group (Fig. 8A and B). Stroke itself is characterized by remarkable inflammation (Anrather and Iadecola, 2016), but these results suggest that MANF may modulate response to a virus or increase infiltration of immune cells. Interestingly, such differences in immune response towardsthe virus were not observed when the transcriptomics experiment was performed using AAV7 instead of AAV1, indicating that the phenomenon may be specific for serotype 1 (Fig. 8D). Different AAV serotypes have different tissue transduction capabilities and lead to different expression levels in different time frames (Zincarelli et al., 2008), which could explain the differences in the response, but this requires further investigation. Many of the genes upregulated in the AAV-MANF group compared to the AAV-eGFP group are associated with defense response to (double-stranded) RNA viruses, whereas the AAV genome in our vectors consists of double-stranded DNA. Thus, it is possible that the changes are virus-independent. Traditionally, AAVs have been considered to be of low immunogenicity (Zaiss and Muruve, 2005), which makes it surprising that the differences can be seen despite the inflammation and other changes induced by stroke.

Regardless of the cause of the changes, in light of these results parenchymal MANF appears to have immunomodulatory effects, which is in line with previous research (Mätlik et al., 2018; Neves et al., 2016; Hartman et al., 2019). According to our results, MANF reverses the stroke-induced upregulation of the proteins S100A8 and S100A9 (Fig. 9A), further evidencing the immunomodulation by MANF. RNA sequencing (Fig. 9B) and qPCR (Fig. 9C) of *S100a8* and *S100a9* transcripts pointed towards the same direction, albeit without statistical significance. S100A8 and S100A9 form a heterodimer calprotectin, but have independent functions as well (Donato et al., 2013). They are well-characterized as a damage-associated molecular pattern (DAMP) in the CNS (Rayasam et al., 2018), involved in phagocyte recruitment and released from phagocytes during activation (Frosch et al., 2000; Rammes et al., 1997). S100A8 and S100A9 have been shown to be induced in the peri-infarct region by focal cerebral ischemia and mediate central nervous system injury via inflammation (Ziegler et al., 2009). Acting as activators of TLR4 (Vogl et al., 2007), they induce proinflammatory cytokines such as TNF-α and IL-8 via NF-κB activation. Notably, these proteins share common mechanisms with some of the stroke-induced changes presented earlier: lysoPC (Fig. 7E) produced by cytosolic phospholipase A_2 ($cPLA_2$) has been shown to be a signal for phagocyte recruitment in the mouse brain (Zhang et al., 2007), and recent evidence suggests that PRDX6 (Fig. S10C) overexpression downregulates TLR4, the target of S100A8/9, leading to decreased neurogenesis in neural stem cell cultures (Yeo et al., 2019).

With immunohistochemistry, we were able to identify S100A9+ cells with neutrophil-like morphology in the peri-infarct region (Fig. 9D). Furthermore, even though the AAV1-MANF treatment affects the levels of S100A8 and S100A9 (Fig. 9A), the number of $S100A9^+$ cells in the peri-infarct region was unaffected by AAV7-MANF (Fig. 9E and F). The events occurring in the brain after stroke are characterized by recruitment of phagocytic cells (Ritzel et al., 2015), and thus, these data are in line with the literature. Previous work has shown that post-stroke delivery of AAV7-MANF leads to a transient increase of phagocytic myeloid cells in the peri-infarct region (Mätlik et al., 2018), and the neuroprotective effect of MANF has been suggested to be due to alternative activation of microglia (Neves et al., 2016). It is possible that S100A8 and S100A9 represent a link in the cascade mediating the effects of MANF, but this requires further investigation.

5. Conclusions

In conclusion, our results illustrate the molecular fingerprint occurring in the ischemic stroke peri-infarct area, in which the endogenous recovery mechanisms operate, at 4 days post-stroke, the time point at which these mechanisms are activated. The multiomics approach utilized in this study yielded complementary data, different omics levels validating each other and making the picture more comprehensive about the biological phenomena discussed in this work. In addition, we characterized the effects of post-stroke AAV1-MANF administration in the peri-infarct region on the transcript, protein, and metabolite level. While no statistically significant changes between the animals treated with AAV-MANF and AAV-eGFP were identified in the metabolomics data, proteomics and transcriptomics data show changes in genes related to immune response. Whether these changes have functional consequences in the biological context, needs further investigation. MANF causes the downregulation of secreted phagocyte proteins S100A8 and S100A9, pointing towards its possible effect on the number or activation of phagocytes in the peri-infarct region. The transcripts related to immune response, especially to the virus, were upregulated in the MANF group, suggesting that it may affect the immune response to the AAV1 vector. While all of these results require further validation, they reinforce the previous findings about the immunomodulatory effects of MANF.

Declarations of Competing Interest

None.

Funding

This study was supported by Business Finland (Tekes; project no. 40395/13, 3iRegeneration), Academy of Finland and Sigrid Juselius Foundation, and the Intramural Program at the National Institute on Drug Abuse, NIH, USA. K.M. was supported by the Ella and Georg Ehrnrooth Foundation and EU FP7 GLORIA (ID No. 602919).

Acknowledgements

The RNA sequencing was carried out at the DNA Sequencing and Genomics Laboratory, Institute of Biotechnology, HiLIFE, University of Helsinki, and the proteomics analysis at the Institute of Biotechnology Proteomics Unit supported by HiLIFE, University of Helsinki and Biocenter Finland.

Appendix A. Supplementary data

Supplementary data to this article can be found online at https://doi.org/10.1016/j.expneurol.2020.113288.

References

Abdullahi, W., Tripathi, D., Ronaldson, P.T., 2018. Blood-brain barrier dysfunction in ischemic stroke: targeting tight junctions and transporters for vascular protection. Am. J. Physiol. Cell Physiol. 315, C343–C356. https://doi.org/10.1152/ajpcell.00095.2018.

Adibhatla, R.M., Hatcher, J.F., Dempsey, R.J., 2006. Lipids and lipidomics in brain injury and diseases. AAPS J. 8, E314–E321. https://doi.org/10.1007/bf02854902.

Airavaara, M., Shen, H., Kuo, C.-C., Peränen, J., Saarma, M., Hoffer, B., Wang, Y., 2009. Mesencephalic astrocyte-derived neurotrophic factor reduces ischemic brain injury and promotes behavioral recovery in rats. J. Comp. Neurol. 515, 116–124. https://doi.org/10.1002/cne.22039.

Airavaara, M., Chiocco, M.J., Howard, D.B., Zuchowski, K.L., Peränen, J., Liu, C., Fang, S., Hoffer, B.J., Wang, Y., Harvey, B.K., 2010. Widespread cortical expression of MANF by AAV serotype 7: localization and protection against ischemic brain injury. Exp. Neurol. 225, 104–113. https://doi.org/10.1016/j.expneurol.2010.05.020.

Airavaara, M., Pickens, C.L., Stern, A.L., Wihbey, K.A., Harvey, B.K., Bossert, J.M., Liu, Q.-

R., Hoffer, B.J., Shaham, Y., 2011. Endogenous GDNF in ventral tegmental area and nucleus accumbens does not play a role in the incubation of heroin craving. Addict. Biol. 16, 261–272. https://doi.org/10.1111/j.1369-1600.2010.00281.x.
Anrather, J., Iadecola, C., 2016. Inflammation and stroke: an overview. Neurotherapeutics 13, 661–670. https://doi.org/10.1007/s13311-016-0483-x.
Anttila, J.E., Albert, K., Wires, E.S., Mätlik, K., Loram, L.C., Watkins, L.R., Rice, K.C., Wang, Y., Harvey, B.K., Airavaara, M., 2018. Post-stroke intranasal (+)-naloxone delivery reduces microglial activation and improves behavioral recovery from ischemic injury. eNeuro 5, e0317–e0395. https://doi.org/10.1523/ENEURO.0395-17.2018.
Apostolou, A., Shen, Y., Liang, Y., Luo, J., Fang, S., 2008. Armet, a UPR-upregulated protein, inhibits cell proliferation and ER stress-induced cell death. Exp. Cell Res. 314, 2454–2467. https://doi.org/10.1016/j.yexcr.2008.05.001.
Bai, M., Vozdek, R., Hnizda, A., Jiang, C., Wang, B., Kuchar, L., Li, T., Zhang, Y., Wood, C., Feng, L., Dang, Y., Ma, D.K., 2018. Conserved roles of *C. elegans* and human MANFs in sulfatide binding and cytoprotection. Nat. Commun. 9, 897. https://doi.org/10.1038/s41467-018-03355-0.
Benjamin, E.J., Muntner, P., Alonso, A., Bittencourt, M.S., Callaway, C.W., Carson, A.P., Chamberlain, A.M., Chang, A.R., Cheng, S., Das, S.R., Delling, F.N., Djousse, L., Elkind, M.S.V., Ferguson, J.F., Fornage, M., Jordan, L.C., Khan, S.S., Kissela, B.M., Knutson, K.L., Kwan, T.W., Lackland, D.T., Lewis, T.T., Lichtman, J.H., Longenecker, C.T., Loop, M.S., Lutsey, P.L., Martin, S.S., Matsushita, K., Moran, A.E., Mussolino, M.E., O'Flaherty, M., Pandey, A., Perak, A.M., Rosamond, W.D., Roth, G.A., Sampson, U.K.A., Satou, G.M., Schroeder, E.B., Shah, S.H., Spartano, N.L., Stokes, A., Tirschwell, D.L., Tsao, C.W., Turakhia, M.P., VanWagner, L.B., Wilkins, J.T., Wong, S.S., Virani, S.S., 2019. Heart disease and stroke statistics - 2019 update: a report from the American Heart Association. Circulation 139, e56–e528. https://doi.org/10.1161/CIR.0000000000000659.
Benjamini, Y., Hochberg, Y., 1995. Controlling the false discovery rate: a practical and powerful approach to multiple testing. J. R. Stat. Soc. Ser. B 57, 289–300. https://doi.org/10.2307/2346101.
Bolger, A.M., Lohse, M., Usadel, B., 2014. Trimmomatic: a flexible trimmer for Illumina sequence data. Bioinformatics 30, 2114–2120. https://doi.org/10.1093/bioinformatics/btu170.
Bootman, M.D., Berridge, M.J., Roderick, H.L., 2002. Calcium signalling: more messengers, more channels, more complexity. Curr. Biol. 12, R563–R565. https://doi.org/10.1016/s0960-9822(02)01055-2.
Brea, D., Agulla, J., Staes, A., Gevaert, K., Campos, F., Sobrino, T., Blanco, M., Davalos, A., Castillo, J., Ramos-Cabrer, P., 2015. Study of protein expression in Peri-infarct tissue after cerebral ischemia. Sci. Rep. 5, 12030. https://doi.org/10.1038/srep12030.
Brown, C.E., Li, P., Boyd, J.D., Delaney, K.R., Murphy, T.H., 2007. Extensive turnover of dendritic spines and vascular remodeling in cortical tissues recovering from stroke. J. Neurosci. 27, 4101–4109. https://doi.org/10.1523/JNEUROSCI.4295-06.2007.
Brown, C.E., Aminoltejari, K., Erb, H., Winship, I.R., Murphy, T.H., 2009. In vivo voltage-sensitive dye imaging in adult mice reveals that somatosensory maps lost to stroke are replaced over weeks by new structural and functional circuits with prolonged modes of activation within both the peri-infarct zone and distant sites. J. Neurosci. 29, 1719–1734. https://doi.org/10.1523/JNEUROSCI.4249-08.2009.
Brown, G.R., Hem, V., Katz, K.S., Ovetsky, M., Wallin, C., Ermolaeva, O., Tolstoy, I., Tatusova, T., Pruitt, K.D., Maglott, D.R., Murphy, T.D., 2015. Gene: a gene-centered information resource at NCBI. Nucleic Acids Res. 43, D36–D42. https://doi.org/10.1093/nar/gku1055.
Cox, J., Mann, M., 2008. MaxQuant enables high peptide identification rates, individualized p.p.b.-range mass accuracies and proteome-wide protein quantification. Nat. Biotechnol. 26, 1367–1372. https://doi.org/10.1038/nbt.1511.
Cox, J., Neuhauser, N., Michalski, A., Scheltema, R.A., Olsen, J.V., Mann, M., 2011. Andromeda: a peptide search engine integrated into the MaxQuant environment. J. Proteome Res. 10, 1794–1805. https://doi.org/10.1021/pr101065j.
Demougeot, C., Marie, C., Giroud, M., Beley, A., 2004. N-acetylaspartate: a literature review of animal research on brain ischaemia. J. Neurochem. 90, 776–783. https://doi.org/10.1111/j.1471-4159.2004.02583.x.
Dobin, A., Davis, C.A., Schlesinger, F., Drenkow, J., Zaleski, C., Jha, S., Batut, P., Chaisson, M., Gingeras, T.R., 2013. STAR: ultrafast universal RNA-seq aligner. Bioinformatics 29, 15–21. https://doi.org/10.1093/bioinformatics/bts635.
Donato, R., Cannon, B.R., Sorci, G., Riuzzi, F., Hsu, K., Weber, D.J., Geczy, C.L., 2013. Functions of S100 proteins. Curr. Mol. Med. 13, 24–57.
Dührkop, K., Shen, H., Meusel, M., Rousu, J., Böcker, S., 2015. Searching molecular structure databases with tandem mass spectra using CSI:FingerID. Proc. Natl. Acad. Sci. U. S. A. 112, 12580–12585. https://doi.org/10.1073/pnas.1509788112.
Eady, T.N., Khoutorova, L., Atkins, K.D., Bazan, N.G., Belayev, L., 2012. Docosahexaenoic acid complexed to human albumin in experimental stroke: neuroprotective efficacy with a wide therapeutic window. Exp. Transl. Stroke Med. 4, 19. https://doi.org/10.1186/2040-7378-4-19.
Eady, T.N., Khoutorova, L., Obenaus, A., Mohd-Yusof, A., Bazan, N.G., Belayev, L., 2014. Docosahexaenoic acid complexed to albumin provides neuroprotection after experimental stroke in aged rats. Neurobiol. Dis. 62, 1–7. https://doi.org/10.1016/j.nbd.2013.09.008.
Feigin, V.L., Forouzanfar, M.H., Krishnamurthi, R., Mensah, G.A., Connor, M., Bennett, D.A., Moran, A.E., Sacco, R.L., Anderson, L., Truelsen, T., O'Donnell, M., Venketasubramanian, N., Barker-Collo, S., Lawes, C.M.M., Wang, W., Shinohara, Y., Witt, E., Ezzati, M., Naghavi, M., Murray, C., 2014. Global and regional burden of stroke during 1990-2010: findings from the Global Burden of Disease Study 2010. Lancet (London, England) 383, 245–254. https://doi.org/10.1016/s0140-6736(13)61953-4.
Frasch, S.C., Bratton, D.L., 2012. Emerging roles for lysophosphatidylserine in resolution of inflammation. Prog. Lipid Res. 51, 199–207. https://doi.org/10.1016/j.plipres.2012.03.001.
Frosch, M., Strey, A., Vogl, T., Wulffraat, N.M., Kuis, W., Sunderkötter, C., Harms, E., Sorg, C., Roth, J., 2000. Myeloid-related proteins 8 and 14 are specifically secreted during interaction of phagocytes and activated endothelium and are useful markers for monitoring disease activity in pauciarticular-onset juvenile rheumatoid arthritis. Arthritis Rheum. 43, 628–637. https://doi.org/10.1002/1529-0131(200003)43:3<628::AID-ANR20>3.0.CO;2-X.
Gal-Oz, S.T., Maier, B., Yoshida, H., Seddu, K., Elbaz, N., Czysz, C., Zuk, O., Stranger, B.E., Ner-Gaon, H., Shay, T., 2019. ImmGen report: sexual dimorphism in the immune system transcriptome. Nat. Commun. 10 (1), 4295. https://doi.org/10.1038/s41467-019-12348-6.
Gesuete, R., Stevens, S.L., Stenzel-Poore, M.P., 2016. Role of circulating immune cells in stroke and preconditioning-induced protection. Acta Neurochir. Suppl. 121, 39–44. https://doi.org/10.1007/978-3-319-18497-5_7.
Guijas, C., Montenegro-Burke, J.R., Domingo-Almenara, X., Palermo, A., Warth, B., Hermann, G., Koellensperger, G., Huan, T., Uritboonthai, W., Aisporna, A.E., Wolan, D.W., Spilker, M.E., Benton, H.P., Siuzdak, G., 2018. METLIN: a technology platform for identifying Knowns and unknowns. Anal. Chem. 90, 3156–3164. https://doi.org/10.1021/acs.analchem.7b04424.
Guyot, L.L., Diaz, F.G., O'Regan, M.H., McLeod, S., Park, H., Phillis, J.W., 2001. Real-time measurement of glutamate release from the ischemic penumbra of the rat cerebral cortex using a focal middle cerebral artery occlusion model. Neurosci. Lett. 299, 37–40. https://doi.org/10.1016/s0304-3940(01)01510-5.
Hadley, G., Neuhaus, A.A., Couch, Y., Beard, D.J., Adriaanse, B.A., Vekrellis, K., DeLuca, G.C., Papadakis, M., Sutherland, B.A., Buchan, A.M., 2018. The role of the endoplasmic reticulum stress response following cerebral ischemia. Int. J. Stroke 13, 379–390. https://doi.org/10.1177/1747493017724584.
Hartman, J.H., Richie, C.T., Gordon, K.L., Mello, D.F., Castillo, P., Zhu, A., Wang, Y., Hoffer, B.J., Sherwood, D.R., Meyer, J.N., Harvey, B.K., 2019. MANF deletion abrogates early larval *Caenorhabditis elegans* stress response to tunicamycin and *Pseudomonas aeruginosa*. Eur. J. Cell Biol. https://doi.org/10.1016/j.ejcb.2019.05.002.
Hellman, M., Arumäe, U., Yu, L., Lindholm, P., Peränen, J., Saarma, M., Permi, P., 2011. Mesencephalic astrocyte-derived neurotrophic factor (MANF) has a unique mechanism to rescue apoptotic neurons. J. Biol. Chem. 286, 2675–2680. https://doi.org/10.1074/jbc.M110.146738.
Huang, D.W., Sherman, B.T., Lempicki, R.A., 2009a. Bioinformatics enrichment tools: paths toward the comprehensive functional analysis of large gene lists. Nucleic Acids Res. 37, 1–13. https://doi.org/10.1093/nar/gkn923.
Huang, D.W., Sherman, B.T., Lempicki, R.A., 2009b. Systematic and integrative analysis of large gene lists using DAVID bioinformatics resources. Nat. Protoc. 4, 44–57. https://doi.org/10.1038/nprot.2008.211.
Imahori, T., Hosoda, K., Nakai, T., Yamamoto, Y., Irino, Y., Shinohara, M., Sato, N., Sasayama, T., Tanaka, K., Nagashima, H., Kohta, M., Kohmura, E., 2017. Combined metabolic and transcriptional profiling identifies pentose phosphate pathway activation by HSP27 phosphorylation during cerebral ischemia. Neuroscience 349, 1–16. https://doi.org/10.1016/j.neuroscience.2017.02.036.
Irie, M., Fujimura, Y., Yamato, M., Miura, D., Wariishi, H., 2014. Integrated MALDI-MS imaging and LC-MS techniques for visualizing spatiotemporal metabolomic dynamics in a rat stroke model. Metabolomics 10, 473–483. https://doi.org/10.1007/s11306-013-0588-8.
Jiao, S., Li, Z., 2011. Non-apoptotic function of BAD and BAX in long-term depression of synaptic transmission. Neuron 70, 758–772. https://doi.org/10.1016/j.neuron.2011.04.004.
Kamat, S.S., Camara, K., Parsons, W.H., Chen, D.-H., Dix, M.M., Bird, T.D., Howell, A.R., Cravatt, B.F., 2015. Immunomodulatory lysophosphatidylserines are regulated by ABHD16A and ABHD12 interplay. Nat. Chem. Biol. 11, 164–171. https://doi.org/10.1038/nchembio.1721.
Kanehisa, M., Goto, S., 2000. KEGG: Kyoto encyclopedia of genes and genomes. Nucleic Acids Res. 28, 27–30. https://doi.org/10.1093/nar/28.1.27.
Kashkar, H., Wiegmann, K., Yazdanpanah, B., Haubert, D., Krönke, M., 2005. Acid sphingomyelinase is indispensable for UV light-induced Bax conformational change at the mitochondrial membrane. J. Biol. Chem. 280, 20804–20813. https://doi.org/10.1074/jbc.M410869200.
Kinuta, Y., Kimura, M., Itokawa, Y., Ishikawa, M., Kikuchi, H., 1989. Changes in xanthine oxidase in ischemic rat brain. J. Neurosurg. 71, 417–420. https://doi.org/10.3171/jns.1989.71.3.0417.
Kopylova, E., Noe, L., Touzet, H., 2012. SortMeRNA: fast and accurate filtering of ribosomal RNAs in metatranscriptomic data. Bioinformatics 28, 3211–3217. https://doi.org/10.1093/bioinformatics/bts611.
Krebs, J., Agellon, L.B., Michalak, M., 2015. Ca(2+) homeostasis and endoplasmic reticulum (ER) stress: an integrated view of calcium signaling. Biochem. Biophys. Res. Commun. 460, 114–121. https://doi.org/10.1016/j.bbrc.2015.02.004.
Lai, T.W., Zhang, S., Wang, Y.T., 2014. Excitotoxicity and stroke: identifying novel targets for neuroprotection. Prog. Neurobiol. 115, 157–188. https://doi.org/10.1016/j.pneurobio.2013.11.006.
Lawrence, M., Huber, W., Pages, H., Aboyoun, P., Carlson, M., Gentleman, R., Morgan, M.T., Carey, V.J., 2013. Software for computing and annotating genomic ranges. PLoS Comput. Biol. 9, e1003118. https://doi.org/10.1371/journal.pcbi.1003118.
Li, P., Murphy, T.H., 2008. Two-photon imaging during prolonged middle cerebral artery occlusion in mice reveals recovery of dendritic structure after reperfusion. J. Neurosci. 28, 11970–11979. https://doi.org/10.1523/JNEUROSCI.3724-08.2008.
Li, F., Silva, M.D., Sotak, C.H., Fisher, M., 2000. Temporal evolution of ischemic injury evaluated with diffusion-, perfusion-, and T2-weighted MRI. Neurology 54, 689–696. https://doi.org/10.1212/wnl.54.3.689.
Li, S., Nie, E.H., Yin, Y., Benowitz, L.I., Tung, S., Vinters, H. V, Bahjat, F.R., Stenzel-Poore,

M.P., Kawaguchi, R., Coppola, G., Carmichael, S.T., 2015. GDF10 is a signal for axonal sprouting and functional recovery after stroke. Nat. Neurosci. 18, 1737–1745. doi:https://doi.org/10.1038/nn.4146.
Li, T., Xu, W., Gao, L., Guan, G., Zhang, Z., He, P., Xu, H., Fan, L., Yan, F., Chen, G., 2019. Mesencephalic astrocyte-derived neurotrophic factor affords neuroprotection to early brain injury induced by subarachnoid hemorrhage via activating Akt-dependent prosurvival pathway and defending blood-brain barrier integrity. FASEB J. Off. Publ. Fed. Am. Soc. Exp. Biol. 33, 1727–1741. https://doi.org/10.1096/fj.201800227RR.
Liang, H., Zhao, H., Gleichman, A., Machnicki, M., Telang, S., Tang, S., Rshtouni, M., Ruddell, J., Carmichael, S.T., 2019. Region-specific and activity-dependent regulation of SVZ neurogenesis and recovery after stroke. Proc. Natl. Acad. Sci. U. S. A. 116, 13621–13630. https://doi.org/10.1073/pnas.1811825116.
Lindahl, M., Danilova, T., Palm, E., Lindholm, P., Voikar, V., Hakonen, E., Ustinov, J., Andressoo, J.-O., Harvey, B.K., Otonkoski, T., Rossi, J., Saarma, M., 2014. MANF is indispensable for the proliferation and survival of pancreatic beta cells. Cell Rep. 7, 366–375. https://doi.org/10.1016/j.celrep.2014.03.023.
Liu, F., Schafer, D.P., McCullough, L.D., 2009. TTC, fluoro-Jade B and NeuN staining confirm evolving phases of infarction induced by middle cerebral artery occlusion. J. Neurosci. Methods 179, 1–8. https://doi.org/10.1016/j.jneumeth.2008.12.028.
Longo, N., Frigeni, M., Pasquali, M., 2016. Carnitine transport and fatty acid oxidation. Biochim. Biophys. Acta 1863, 2422–2435. https://doi.org/10.1016/j.bbamcr.2016.01.023.
Love, M.I., Huber, W., Anders, S., 2014. Moderated estimation of fold change and dispersion for RNA-seq data with DESeq2. Genome Biol. 15, 550. https://doi.org/10.1186/s13059-014-0550-8.
Mätlik, K., Abo-Ramadan, U., Harvey, B.K., Arumäe, U., Airavaara, M., 2014. AAV-mediated targeting of gene expression to the peri-infarct region in rat cortical stroke model. J. Neurosci. Methods 236, 107–113. https://doi.org/10.1016/j.jneumeth.2014.08.014.
Mätlik, K., Anttila, J.E., Kuan-Yin, T., Smolander, O.-P., Pakarinen, E., Lehtonen, L., Abo-Ramadan, U., Lindholm, P., Zheng, C., Harvey, B., Arumäe, U., Lindahl, M., Airavaara, M., 2018. Poststroke delivery of MANF promotes functional recovery in rats. Sci. Adv. 4https://doi.org/10.1126/sciadv.aap8957. eaap8957.
Merali, Z., Huang, K., Mikulis, D., Silver, F., Kassner, A., 2017. Evolution of blood-brain-barrier permeability after acute ischemic stroke. PLoS One 12, e0171558. https://doi.org/10.1371/journal.pone.0171558.
Moffett, J.R., Ross, B., Arun, P., Madhavarao, C.N., Namboodiri, A.M.A., 2007. N-Acetylaspartate in the CNS: from neurodiagnostics to neurobiology. Prog. Neurobiol. 81, 89–131. https://doi.org/10.1016/j.pneurobio.2006.12.003.
Morimoto, N., Oida, Y., Shimazawa, M., Miura, M., Kudo, T., Imaizumi, K., Hara, H., 2007. Involvement of endoplasmic reticulum stress after middle cerebral artery occlusion in mice. Neuroscience 147, 957–967. https://doi.org/10.1016/J.NEUROSCIENCE.2007.04.017.
Moskowitz, M.A., Lo, E.H., Iadecola, C., 2010. The science of stroke: mechanisms in search of treatments. Neuron 67, 181–198. https://doi.org/10.1016/j.neuron.2010.07.002.
Mulcahy, N.J., Ross, J., Rothwell, N.J., Loddick, S.A., 2003. Delayed administration of interleukin-1 receptor antagonist protects against transient cerebral ischaemia in the rat. Br. J. Pharmacol. 140, 471–476. https://doi.org/10.1038/sj.bjp.0705462.
Nakka, V.P., Prakash-Babu, P., Vemuganti, R., 2016. Crosstalk between endoplasmic reticulum stress, oxidative stress, and autophagy: potential therapeutic targets for acute CNS injuries. Mol. Neurobiol. 53, 532–544. https://doi.org/10.1007/s12035-014-9029-6.
Narita, K., Kubota, M., Nakane, M., Kitahara, S., Nakagomi, T., Tamura, A., Hisaki, H., Shimasaki, H., Ueta, N., 2000. Therapeutic time window in the penumbra during permanent focal ischemia in rats: changes of free fatty acids and glycerophospholipids. Neurol. Res. 22, 393–400. https://doi.org/10.1080/01616412.2000.11740689.
Neves, J., Zhu, J., Sousa-Victor, P., Konjikusic, M., Riley, R., Chew, S., Qi, Y., Jasper, H., Lamba, D.A., 2016. Immune modulation by MANF promotes tissue repair and regenerative success in the retina. Science 353https://doi.org/10.1126/science.aaf3646. aaf3646.
Oslowski, C.M., Urano, F., 2011. Measuring ER stress and the unfolded protein response using mammalian tissue culture system. Methods Enzymol. 490, 71–92. https://doi.org/10.1016/B978-0-12-385114-7.00004-0.
Pello, S., Boland, T., Dechant, V., Patel, S., Liang, T.-W., Mandel, S., 2009. Uric Acid's relationship with stroke and Parkinson's disease: a review - practical neurology. Pract. Neurol. 8, 21–23.
Pluskal, T., Castillo, S., Villar-Briones, A., Oresic, M., 2010. MZmine 2: modular framework for processing, visualizing, and analyzing mass spectrometry-based molecular profile data. BMC Bioinform. 11, 395. https://doi.org/10.1186/1471-2105-11-395.
Powers, W.J., Rabinstein, A.A., Ackerson, T., Adeoye, O.M., Bambakidis, N.C., Becker, K., Biller, J., Brown, M., Demaerschalk, B.M., Hoh, B., Jauch, E.C., Kidwell, C.S., Leslie-Mazwi, T.M., Ovbiagele, B., Scott, P.A., Sheth, K.N., Southerland, A.M., Summers, D. V, Tirschwell, D.L., 2018. 2018 guidelines for the early Management of Patients with Acute Ischemic Stroke: a guideline for healthcare professionals from the American Heart Association/American Stroke Association. Stroke 49, e46–e110. doi:https://doi.org/10.1161/STR.0000000000000158.
Pulfer, M., Murphy, R.C., 2003. Electrospray mass spectrometry of phospholipids. Mass Spectrom. Rev. 22, 332–364. https://doi.org/10.1002/mas.10061.
R Core Team, 2019. R: A Language and Environment for Statistical Computing.
Rammes, A., Roth, J., Goebeler, M., Klempt, M., Hartmann, M., Sorg, C., 1997. Myeloid-related protein (MRP) 8 and MRP14, calcium-binding proteins of the S100 family, are secreted by activated monocytes via a novel, tubulin-dependent pathway. J. Biol. Chem. 272, 9496–9502. https://doi.org/10.1074/jbc.272.14.9496.
Rayasam, A., Hsu, M., Kijak, J.A., Kissel, L., Hernandez, G., Sandor, M., Fabry, Z., 2018. Immune responses in stroke: how the immune system contributes to damage and healing after stroke and how this knowledge could be translated to better cures? Immunology 154, 363–376. https://doi.org/10.1111/imm.12918.
Ritzel, R.M., Patel, A.R., Grenier, J.M., Crapser, J., Verma, R., Jellison, E.R., McCullough, L.D., 2015. Functional differences between microglia and monocytes after ischemic stroke. J. Neuroinflammation 12, 106. https://doi.org/10.1186/s12974-015-0329-1.
Rodhe, J., Burguillos, M.A., de Pablos, R.M., Kavanagh, E., Persson, A., Englund, E., Deierborg, T., Venero, J.L., Joseph, B., 2016. Spatio-temporal activation of caspase-8 in myeloid cells upon ischemic stroke. Acta Neuropathol. Commun. 4, 92. https://doi.org/10.1186/s40478-016-0365-9.
RStudio Team, 2019. RStudio: Integrated Development for R.
Seo, W.-K., Jo, G., Shin, M.-J., Oh, K., 2018. Medium-chain acylcarnitines are associated with cardioembolic stroke and stroke recurrence. Arterioscler. Thromb. Vasc. Biol. 38, 2245–2253. https://doi.org/10.1161/ATVBAHA.118.311373.
Shanshan, Y., Beibei, J., Li, T., Minna, G., Shipeng, L., Li, P., Yong, Z., 2017. Phospholipase A2 of Peroxiredoxin 6 plays a critical role in cerebral ischemia/reperfusion inflammatory injury. Front. Cell. Neurosci. 11, 99. https://doi.org/10.3389/fncel.2017.00099.
Shen, Yujun, Sun, A., Wang, Y., Cha, D., Wang, H., Wang, F., Feng, L., Fang, S., Shen, Yuxian, 2012. Upregulation of mesencephalic astrocyte-derived neurotrophic factor in glial cells is associated with ischemia-induced glial activation. J. Neuroinflammation 9, 254. https://doi.org/10.1186/1742-2094-9-254.
Shen, H., Dührkop, K., Böcker, S., Rousu, J., 2014. Metabolite identification through multiple kernel learning on fragmentation trees. Bioinformatics 30, i157–i164. https://doi.org/10.1093/bioinformatics/btu275.
Subramanian, A., Tamayo, P., Mootha, V.K., Mukherjee, S., Ebert, B.L., Gillette, M.A., Paulovich, A., Pomeroy, S.L., Golub, T.R., Lander, E.S., Mesirov, J.P., 2005 Oct 25. Gene set enrichment analysis: a knowledge-based approach for interpreting genome-wide expression profiles. Proc. Natl. Acad. Sci. U. S. A. 102 (43), 15545–15550 Epub 2005 Sep 30. PubMed PMID: 16199517; PubMed Central PMCID: PMC1239896.
Sud, M., Fahy, E., Cotter, D., Brown, A., Dennis, E.A., Glass, C.K., Merrill, A.H.J., Murphy, R.C., Raetz, C.R.H., Russell, D.W., Subramaniam, S., 2007. LMSD: LIPID MAPS structure database. Nucleic Acids Res. 35, D527–D532. https://doi.org/10.1093/nar/gkl838.
Taha, T.A., Mullen, T.D., Obeid, L.M., 2006. A house divided: ceramide, sphingosine, and sphingosine-1-phosphate in programmed cell death. Biochim. Biophys. Acta 1758, 2027–2036. https://doi.org/10.1016/j.bbamem.2006.10.018.
Talman, V., Teppo, J., Pöhö, P., Movahedi, P., Vaikkinen, A., Karhu, S.T., Trošt, K., Suvitaival, T., Heikkonen, J., Pahikkala, T., Kotiaho, T., Kostiainen, R., Varjosalo, M., Ruskoaho, H., 2018. Molecular atlas of postnatal mouse heart development. J. Am. Heart Assoc. 7, e010378. https://doi.org/10.1161/JAHA.118.010378.
The Gene Ontology Consortium, 2017. Expansion of the gene ontology knowledgebase and resources. Nucleic Acids Res. 45, D331–D338. https://doi.org/10.1093/nar/gkw1108.
The Gene Ontology Consortium, 2019. The gene ontology resource: 20 years and still GOing strong. Nucleic Acids Res. 47, D330–D338. https://doi.org/10.1093/nar/gky1055.
Tseng, K.-Y., Danilova, T., Domanskyi, A., Saarma, M., Lindahl, M., Airavaara, M., 2017. MANF is essential for Neurite extension and neuronal migration in the developing cortex. eNeuro 4, e0214–e0217. https://doi.org/10.1523/ENEURO.0214-17.2017.
Tseng, K.-Y., Anttila, J.E., Khodosevich, K., Tuominen, R.K., Lindahl, M., Domanskyi, A., Airavaara, M., 2018. MANF promotes differentiation and migration of neural progenitor cells with potential neural regenerative effects in stroke. Mol. Ther. 26, 238–255. https://doi.org/10.1016/j.ymthe.2017.09.019.
Uemura, Y., Miller, J.M., Matson, W.R., Beal, M.F., 1991. Neurochemical analysis of focal ischemia in rats. Stroke 22, 1548–1553. https://doi.org/10.1161/01.str.22.12.1548.
UniProt Consortium, 2019. UniProt: a worldwide hub of protein knowledge. Nucleic Acids Res. 47, D506–D515. https://doi.org/10.1093/nar/gky1049.
Van Wylen, D.G., Park, T.S., Rubio, R., Berne, R.M., 1986. Increases in cerebral interstitial fluid adenosine concentration during hypoxia, local potassium infusion, and ischemia. J. Cereb. Blood Flow Metab. 6, 522–528. https://doi.org/10.1038/jcbfm.1986.97.
Vogl, T., Tenbrock, K., Ludwig, S., Leukert, N., Ehrhardt, C., van Zoelen, M.A.D., Nacken, W., Foell, D., van der Poll, T., Sorg, C., Roth, J., 2007. Mrp8 and Mrp14 are endogenous activators of Toll-like receptor 4, promoting lethal, endotoxin-induced shock. Nat. Med. 13, 1042–1049. https://doi.org/10.1038/nm1638.
Wang, Y.-P., Zhou, L.-S., Zhao, Y.-Z., Wang, S.-W., Chen, L.-L., Liu, L.-X., Ling, Z.-Q., Hu, F.-J., Sun, Y.-P., Zhang, J.-Y., Yang, C., Yang, Y., Xiong, Y., Guan, K.-L., Ye, D., 2014. Regulation of G6PD acetylation by SIRT2 and KAT9 modulates NADPH homeostasis and cell survival during oxidative stress. EMBO J. 33, 1304–1320. https://doi.org/10.1002/embj.201387224.
Weigert, A., Olesch, C., Brüne, B., 2019. Sphingosine-1-phosphate and macrophage biology-how the Sphinx tames the big eater. Front. Immunol. 10, 1706. https://doi.org/10.3389/fimmu.2019.01706.
Wishart, D.S., Feunang, Y.D., Marcu, A., Guo, A.C., Liang, K., Vazquez-Fresno, R., Sajed, T., Johnson, D., Li, C., Karu, N., Sayeeda, Z., Lo, E., Assempour, N., Berjanskii, M., Singhal, S., Arndt, D., Liang, Y., Badran, H., Grant, J., Serra-Cayuela, A., Liu, Y., Mandal, R., Neveu, V., Pon, A., Knox, C., Wilson, M., Manach, C., Scalbert, A., 2018. HMDB 4.0: the human metabolome database for 2018. Nucleic Acids Res. 46, D608–D617. https://doi.org/10.1093/nar/gkx1089.
Yan, Y., Rato, C., Rohland, L., Preissler, S., Ron, D., 2019. MANF antagonizes nucleotide exchange by the endoplasmic reticulum chaperone BiP. Nat. Commun. 10, 541. https://doi.org/10.1038/s41467-019-08450-4.
Yang, W., Paschen, W., 2016. Unfolded protein response in brain ischemia: a timely update. J. Cereb. Blood Flow Metab. 36, 2044–2050. https://doi.org/10.1177/0271678X16674488.

Yang, Y., Zhong, Q., Mo, C., Zhang, H., Zhou, T., Tan, W., 2017. Determination of endogenous inflammation-related lipid mediators in ischemic stroke rats using background subtracting calibration curves by liquid chromatography-tandem mass spectrometry. Anal. Bioanal. Chem. 409, 6537–6547. https://doi.org/10.1007/s00216-017-0600-7.

Yeo, I.J., Park, M.H., Son, D.J., Kim, J.Y., Nam, K.T., Hyun, B.K., Kim, S.Y., Jung, M.H., Song, M.J., Chun, H.O., Lee, T.H., Han, S.-B., Hong, J.T., 2019. PRDX6 inhibits neurogenesis through Downregulation of WDFY1-mediated TLR4 signal. Mol. Neurobiol. 56, 3132–3144. https://doi.org/10.1007/s12035-018-1287-2.

Yoshida, S., Inoh, S., Asano, T., Sano, K., Kubota, M., Shimazaki, H., Ueta, N., 1980. Effect of transient ischemia on free fatty acids and phospholipids in the gerbil brain. Lipid peroxidation as a possible cause of postischemic injury. J. Neurosurg. 53, 323–331. https://doi.org/10.3171/jns.1980.53.3.0323.

Yu, J., Novgorodov, S.A., Chudakova, D., Zhu, H., Bielawska, A., Bielawski, J., Obeid, L.M., Kindy, M.S., Gudz, T.I., 2007. JNK3 signaling pathway activates ceramide synthase leading to mitochondrial dysfunction. J. Biol. Chem. 282, 25940–25949. https://doi.org/10.1074/jbc.M701812200.

Yu, Y.-Q., Liu, L.-C., Wang, F.-C., Liang, Y., Cha, D.-Q., Zhang, J.-J., Shen, Y.-J., Wang, H.-P., Fang, S., Shen, Y.-X., 2010. Induction profile of MANF/ARMET by cerebral ischemia and its implication for neuron protection. J. Cereb. Blood Flow Metab. 30, 79–91. https://doi.org/10.1038/jcbfm.2009.181.

Yui, S., Nakatani, Y., Mikami, M., 2003. Calprotectin (S100A8/S100A9), an inflammatory protein complex from neutrophils with a broad apoptosis-inducing activity. Biol. Pharm. Bull. 26, 753–760. https://doi.org/10.1248/bpb.26.753.

Zaiss, A.K., Muruve, D.A., 2005. Immune responses to adeno-associated virus vectors. Curr. Gene Ther. 5, 323–331.

Zhang, Z., Lee, Y.-C., Kim, S.-J., Choi, M.S., Tsai, P.-C., Saha, A., Wei, H., Xu, Y., Xiao, Y.-J., Zhang, P., Heffer, A., Mukherjee, A.B., 2007. Production of lysophosphatidylcholine by cPLA2 in the brain of mice lacking PPT1 is a signal for phagocyte infiltration. Hum. Mol. Genet. 16, 837–847. https://doi.org/10.1093/hmg/ddm029.

Zhang, Y., Chen, K., Sloan, S.A., Bennett, M.L., Scholze, A.R., O'Keeffe, S., Phatnani, H.P., Guarnieri, P., Caneda, C., Ruderisch, N., Deng, S., Liddelow, S.A., Zhang, C., Daneman, R., Maniatis, T., Barres, B.A., Wu, J.Q., 2014. An RNA-sequencing transcriptome and splicing database of glia, neurons, and vascular cells of the cerebral cortex. J. Neurosci. 34 (36), 11929–11947. https://doi.org/10.1523/JNEUROSCI.1860-14.2014.

Ziegler, G., Prinz, V., Albrecht, M.W., Harhausen, D., Khojasteh, U., Nacken, W., Endres, M., Dirnagl, U., Nietfeld, W., Trendelenburg, G., 2009. Mrp-8 and -14 mediate CNS injury in focal cerebral ischemia. Biochim. Biophys. Acta 1792, 1198–1204. https://doi.org/10.1016/j.bbadis.2009.10.003.

Zincarelli, C., Soltys, S., Rengo, G., Rabinowitz, J.E., 2008. Analysis of AAV serotypes 1-9 mediated gene expression and tropism in mice after systemic injection. Mol. Ther. 16, 1073–1080. https://doi.org/10.1038/mt.2008.76.